Modeling simulation of aerosol light absorption over the Beijing-Tianjin-Hebei region: the impact of mixing state and aging processes

Huiyun Du[1,2], Jie Li[1,2,3*], Xueshun Chen[1,2*], Gabriele Curci[4], Fangqun Yu[5], Yele Sun[1,2], Xu Dao[6], Song Guo[7], Zhe Wang[1,2], Wenyi Yang[8], Lianfang Wei[9], Zifa Wang[1,2,3]

[1]State Key Laboratory of Atmospheric Environment and Extreme Meteorology, Institute of Atmospheric Physics, Chinese Academy of Sciences, Beijing 100029, China
[2]State Key Laboratory of Atmospheric Boundary Layer Physics and Atmospheric Chemistry (LAPC), Institute of Atmospheric Physics, Chinese Academy of Sciences, Beijing 100029, China
[3]College of Earth and Planetary Sciences, University of Chinese Academy of Sciences, Beijing 100049, China
[4]Department of Physical and Chemical Sciences, University of L'Aquila, L'Aquila, Italy
[5]Atmospheric Sciences Research Centre, University at Albany, Albany, NY, USA
[6]China National Environmental Monitoring Centre, Beijing 100012, China
[7]College of Environmental Sciences and Engineering, Peking University, Beijing 100871, China
[8]Center of Environmental Pollution and Greenhouse Gases Co-control, Chinese Academy of Environmental Planning, Beijing 100041, China
[9]Chinese Research Academy of Environmental Sciences, Beijing 100012, China

Correspondence to: Jie Li (lijie8074@mail.iap.ac.cn), Xueshun Chen (chenxsh@mail.iap.ac.cn)

Abstract. The mixing state and aging characteristics of black carbon (BC) aerosols are the key factors in calculating their optical properties and quantifying their impacts on radiation balance and global climate change. Considerable uncertainty still exists in the absorption properties of BC-containing aerosols and the absorption enhancement (E_{abs}) due to the lensing effect. It is crucial to reasonably represent the mixing of BC with other aerosol components to reduce this uncertainty. In this study, the absorption properties of $PM_{2.5}$ were investigated based on the nested air quality prediction model system (NAQPMS) with different assumptions of the aerosol mixing state. The absorption coefficient (b_{abs}) is highest under uniform internal mixing, lower under core-shell mixing, and lowest under the assumption of external mixing. The result under core-shell mixing is closest to the observation. The aging process and coating thickness were well reproduced by the advanced particle microphysical module (APM) in NAQPMS. Then the fraction of embedded BC and secondary components coating aerosols was used to constrain the mixing state. The E_{abs} at 880 nm over the Beijing-Tianjin-Hebei region was 2.0~2.5 under core-shell mixing. When the fraction of coated BC and the coating layer are resolved, the E_{abs_880} caused by the lensing effect decreases by 30~43% to 1.2~1.7, which is close to the range reported in previous studies. This study highlights the importance of representing the microphysical processes governing the mixing state and aging of BC and provides a reference for quantifying its radiative effects.
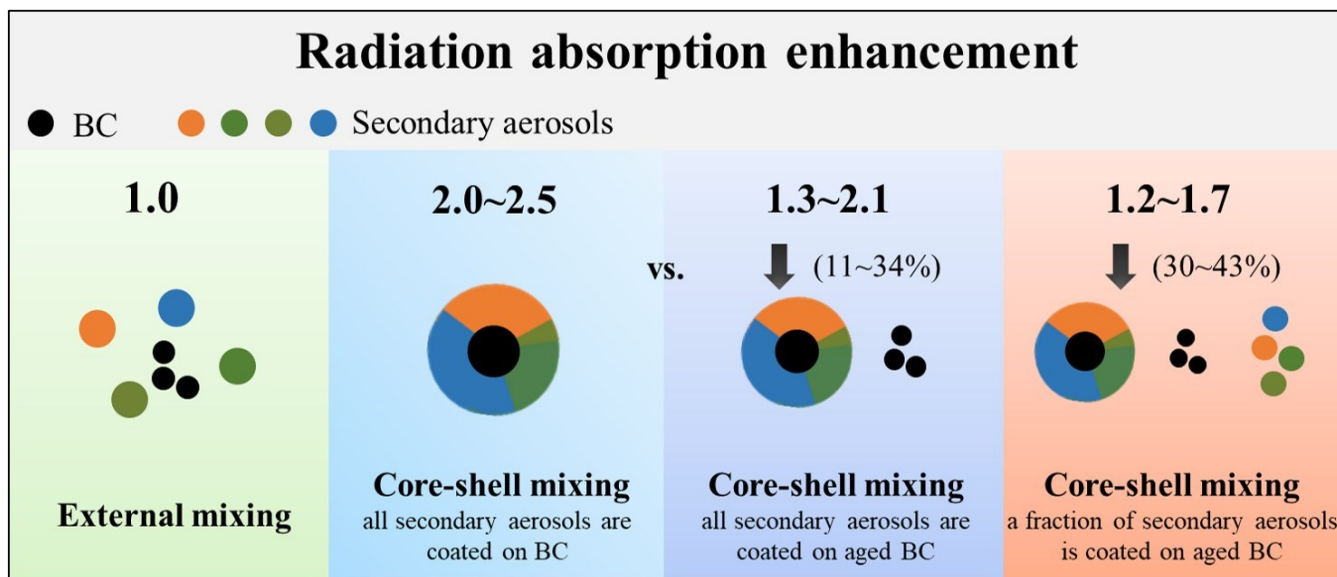
Abstract figure

1 Introduction

35   Aerosols have important environmental and climatic effects, affecting not only transportation and public health but also the global radiation balance (Xu et al., 2013; IPCC, 2021). Mainly originating from incomplete burning, black carbon (BC) is an important component of aerosols. The light absorption of BC particles is enhanced by the "lensing effect" of coating, which affects the heating of the atmosphere by BC (Fuller et al., 1999). When BC is coated by hydrophilic components, it can act as cloud condensation nuclei affecting cloud and rainfall. Previous studies have demonstrated the important radiative forcing

40   effect of BC (Jacobson, 2013; Bond et al., 2013). However, uncertainty in calculating the optical parameters of BC-containing aerosols still exists. It is challenging to quantify the radiative effect of BC.

The mixing state describes the distribution of properties across a population of particles (Riemer et al., 2019). Externally mixed means that each particle in a population is composed of a single species. Internally mixed means that each particle in the population consists of the same mixture of all chemical species (Stevens and Dastoor, 2019). The concept

45   maps illustrating the mixing state are shown in Matsui et al. (2018, Figure 4) and Fierce et al. (2017, Figure 1). The aerosol mixing state is dynamic and changes due to several processes, such as emission, new particle formation, transport, condensation, and coagulation processes (Chen et al., 2023). Purely internal and external mixing states are rare in the real atmosphere (Bondy et al., 2018). In addition, observations have shown that not all BC particles are coated, and not all secondary aerosols are coated on BC cores (Li et al., 2016). Transmission electron microscopy has shown that only a

50   proportion of BC aerosols are embedded (Wang et al., 2021b). The fraction of thickly coated BC in Beijing in winter reduced from 48% to 29% from 2012 to 2018 (Wu et al., 2021). The presentation of aerosol mixing states in atmospheric

models at different scales was highlighted by Riemer et al. (2019). In many models, aerosols are presented in a few modes with assumed size distribution and the same mixing state and compositions in a mode (Liu et al., 2016; Mann et al., 2010). The sectional approach is used in limited models to represent the mixing state (Yu et al., 2012; Matsui et al., 2014; Matsui, 2016; Yu et al., 2015). Furthermore, particle-resolved models can accurately simulate BC mixing states, but it is applied only to the box and single-column models due to the high computational cost (Riemer et al., 2009; Zaveri et al., 2010; Curtis et al., 2017). Yao et al. (2022) verified the important yet complicated role of mixing state in governing aerosol optical properties using an ensemble of 1800 aerosol populations from particle-resolved simulations. Trade off the detail presentation and computational cost, most chemical transport models typically simplify aerosol representation by tracking separate aerosol populations rather than individual particle components (Riemer et al., 2019). Mie theory based on a simple fixed mixing state (external, fully internal, or core-shell mixing) assumption is often used in chemical transport models (Li et al., 2020; Gao et al., 2020).

Comparison between different mixing states conducted in previous studies showed that the BC absorbing properties are sensitive to the mixing state assumptions. Curci et al. (2019) found that aerosol optical depth (AOD) is mainly determined by the aerosol mass and only secondarily affected by the mixing state, however, the absorption enhancement (E_{abs}) values depended on the mixing assumption made in the model. The underestimation in modeled absorption AOD decreased from 66% in the external mixing case to 43% in the core-shell mixing case (Tuccella et al. 2020). Partial internal mixing is the most likely mixing state of aerosols. The fraction of internally mixed particles can be calculated using the parameterization of Cheng et al. (2012) and Curci et al. (2019). The fraction of core-shell can be parameterized as a function of the bulk volume ratio (Hu et al., 2022). The mixing state index and mass ratio of coating to BC were used to improve the BC mixing state presentation and aerosol particles in the accumulation mode were partitioned into BC-free and BC-containing particles (Shen et al., 2024). E_{abs} calculated in a partial internal mixing state were approximately 10% lower than those from core-shell mixing simulations (Tuccella et al., 2020). However, quantitative investigations considering the evolution of mixing states based on microphysical properties are limited (Li et al., 2024). Therefore, the fraction of coated BC and the coating fraction of other components based on microphysical processes should be considered in the optical calculation.

Coating thickness and the heterogeneity of the mixing state are proposed to be the main reasons explaining the gap between field observation, lab investigation, and model simulation in light absorption enhancement (Zhao et al., 2021; Fierce et al., 2020; Wang et al., 2021a). The coating fraction significantly influences the absorption of BC particles. The coating thickness of BC particles can be detected by a single-particle soot photometer (SP2), although the lower measurement limits of SP2 typically result in an overestimation of the concentrations of pure BC (Zhao et al. 2020), and the mass ratio of coating to BC core can highly impact absorption enhancement (Liu et al. 2017; Zhao et al., 2021). The black carbon aging process is an important source of uncertainty in the assessment of its contribution to global warming (Wang et al., 2022). Black carbon can be coated by other aerosols, which increases the complexity of optical properties. Kang et al. (2023) showed that the aging of BC at night in the residual layer can be higher than in the daytime and enhance its light absorption. The aging degree and mixing state can change very quickly in a polluted environment (Peng et al., 2016). An inadequate understanding

of the mixing state of BC greatly hinders the assessment of its climate effects (Huang et al., 2023). However, due to this complexity, few three-dimensional (3-D) models sufficiently resolve BC aging processes (Xie et al., 2023; Zhang et al., 2018). A 3-D modeling study found that the aging time of BC varied greatly and showed significant spatial heterogeneity over the polluted areas in China (Chen et al., 2017b).

In this study, the nested air quality prediction model system (NAQPMS) coupled with an advanced particle microphysics module was used to investigate the absorption properties of aerosols over Northern China in November 2018. The simulation of aerosol components was conducted using the 3-D air quality model. Firstly, three ideal mixing states (external, internal mixing, and core-shell mixing) are considered to study the effect of the mixing state by a Flexible Aerosol Optical Depth module based on observation and simulation of $PM_{2.5}$ components. Then, the fraction of coated BC based on the aging degree of BC, the fraction of coating, and the detailed microphysical processes were considered during the absorption calculation. Finally, the impact of aging processes on light absorption enhancement was investigated.

2 Data and methods

2.1 Observation data

The study period is from November 1, 2018, to November 30, 2018. Observations of $PM_{2.5}$ components were obtained from the China National Environmental Monitoring Centre. The observation site in Beijing (BJ), located at the China National Environmental Monitoring Centre (40º2′N, 116º41′E), is a typical urban site. Water soluble species (Na^+, K^+, sulfate, nitrate, ammonium, and Cl^-) in $PM_{2.5}$ were measured by Gas and Aerosol Collector (GAC), and particles were collected by wet denuder and detected by Ion chromatography. Organic carbon (OC) and elemental carbon (EC) are detected using the thermo-optical transmittance method. OC can further be classified into primary organic carbon (POC) and secondary organic carbon (SOC) using the elemental carbon (EC) tracer method (Castro et al., 1999; Zhao et al., 2013). A refined EC tracer method was proposed (Zheng et al., 2015; Lin et al., 2009), and data from the lowest 10% percentile of ambient OC/EC ratios was utilized to estimate the primary OC/EC ratio with the following equations (Figure S1).

$$POC = EC \times (OC/EC)_{pri} + N \tag{1}$$

$$SOC = OC - POC \tag{2}$$

The light extinction parameters were measured at the tower site of the Institute of Atmospheric Physics (IAP), Chinese Academy of Sciences (39°58′28″N, 116°22′16″E) in Beijing. The absorption coefficient at a wavelength of 880 nm was directly measured by a seven-wavelength Aethalometer (AE33, Magee Scientific Corp.) (Sun et al., 2021). A new real-time loading effect compensation algorithm was adopted, which is based on a two-parallel spot measurement of optical absorption (Drinovec et al., 2015). It is worth noting that there may be some uncertainty in the absorption measurement due to the use of the reported multiple-scattering correction factor (Yus-Díez et al., 2021; Qin et al., 2018). The extinction coefficient (b_{ext}, λ=630 nm) of $PM_{2.5}$ was measured by a cavity-attenuated phase shift extinction monitor (CAPS PMext Aerodyne Research

Inc.). The absorption coefficient at 630 nm is derived using a fitted power law relationship at seven wavelengths (Ran et al., 2016). The absorption coefficient at 880 nm was used to analyze the performance of the model as BC is the major contributor to aerosol absorption at 880 nm. $PM_{2.5}$, components, and absorption data were used to evaluate the model performance.

2.2 Air quality model

NAQPMS is a 3-D Eulerian terrain-following chemical transport model developed by the Institute of Atmospheric Physics, Chinese Academy of Sciences (Wang et al., 2001). The NAQPMS model coupled with an advanced particle microphysics module (APM, Yu and Luo, 2009) was used in this study (Chen et al., 2014). NAQPMS includes physical processes such as advection, convection, diffusion, and deposition, and chemistry processes such as gas-phase chemistry, aqueous chemistry, and aerosol processes. A volatility basis set (VBS) framework for secondary organic aerosols (SOA) has been coupled to NAQPMS to improve the performance of SOA (Yang et al., 2019; Chen et al., 2021). The APM module includes microphysical processes like nucleation, condensation, evaporation, and coagulation (Yu and Luo, 2009; Chen et al., 2021). Particles are represented by the sectional bin scheme in the APM. Secondary inorganic particles are distributed by 40 bins covering 0.0012–12 μm. BC and OC are represented using 28 bins, and other primary particles such as dust and sea salt are represented by 4 bins. The evolution of particle size distributions and aging processes of BC due to condensation and coagulation are well reproduced by the model (Chen et al., 2017a; Du et al., 2019).

A two-nested model domain was set up in this study. The parent domain covers Northern China at a resolution of 27 km and the second domain covers Beijing-Tianjin-Hebei and surrounding regions with a resolution of 9 km, see Figure 1. To represent fine vertical structures, 30 vertical levels were adopted, including 17 levels below 2 km. The mesoscale model WRF version 4.0.1 was used to provide meteorological fields for NAQPMS. The initial and boundary conditions for meteorology were provided by NCEP final reanalysis data (FNL) every six hours (https://rda.ucar.edu/datasets/ds083.2/), and the MOZART model provided initial chemical fields. The Multi-resolution Emission Inventory for China (MEIC) developed by Tsinghua University with a resolution of 0.1×0.1° was used (http://meicmodel.org.cn). The base year of the emission inventory was 2017. MEIC covers 10 species including BC, OC, $PM_{2.5}$, PM_{10}, CO, NH_3, SO_2, NOx, CH_4, and VOCs. The configuration of WRF and NAQPMS can be seen in Table S1. The simulation of WRF and NAQPMS started on October 24, 2018, and the first 7 days were set aside as spin-up time.
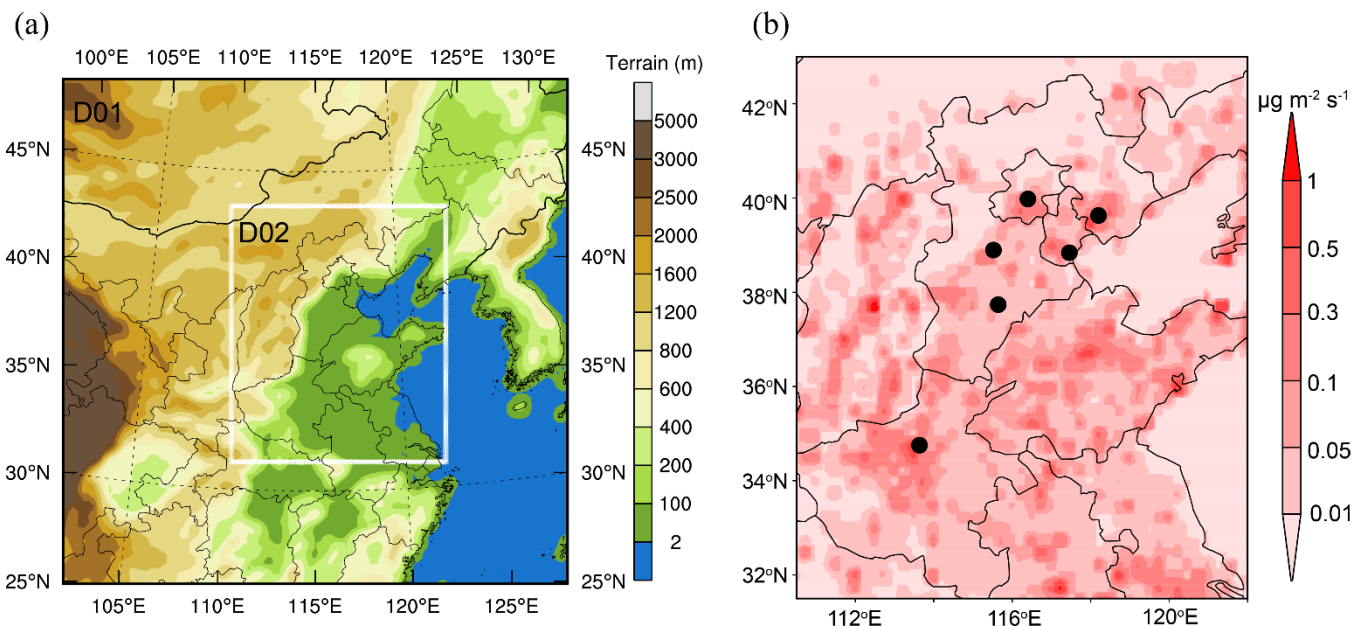
Figure 1. (a) The model domain. (b) Emission rate of primary PM$_{2.5}$ and the location of observation sites. Black dots are pollution sites.

2.2.1 Flexible Aerosol Optical Depth (FlexAOD) module

In this study, the particles are assumed to be spherical and Mie theory (Mie, 1908) is applied to study their optical properties. The FlexAOD (http://pumpkin.aquila.infn.it/flexaod/) (Curci et al., 2015) was employed to calculate extinction and single scatter albedo. The components of PM$_{2.5}$ and relative humidity (RH) are used as input parameters. The average volume of particles for each species is computed by dividing the mass by the species' density. Mixing states considered in the study include the external mixing assumption (EXT), internal homogeneous assumption (HOM), and the core-shell assumption (CS). For the external mixing assumption, extinction is the sum of each species under specific relative humidity. For internal mixing cases (HOM and CS), the particles conform to a lognormal size distribution. For the internal homogeneous assumption, the volume average refractive index is a function of particle size applied over all species. For the core-shell assumption, the refractive index for BC core and homogeneously mixed shell (secondary inorganic aerosols and secondary organic aerosols) are calculated separately. The Mie code based on Toon and Ackerman (1981) is used for the core-shell internal mixing, and the code based on Mishchenko et al. (1999) is adopted for external and homogeneous internal mixing. The size distribution of the different aerosols is taken from the OPAC (Optical Properties of Aerosols and Clouds) database (Hess et al., 1998). The mean diameter of BC is assumed to be 30 nm based on Dentener et al. (2006). The density, complex refractive index, particle hygroscopic growth factor, mean radius, and standard variation of log-normal size distribution are shown in Table S2.

2.2.2 Optical module based on APM

APM is a size-resolved, mixing-state-resolved advanced particle microphysics model coupled in NAQPMS. The mixing state in APM is assumed to be semi-external mixing, which includes internal mixing, external mixing, and core-shell mixing. The seeding particles generated by emission and nucleation (including BC, OC, sulfate, dust, and sea salt) can be coated by secondary particles (including sulfate, nitrate, ammonium, and SOA) through condensation, coagulation, chemical reactions, equilibrium uptake, and hygroscopic growth processes. Sulfate coated by secondary inorganic aerosols (SIA) or SOA is considered to be internal mixing. BC, OC, dust, and sea salt coated with SIA or SOA are considered to be core-shell mixing. These coated particles are externally mixed. The mixing of BC particles with other aerosol components can be well resolved hourly. More details can be seen in Yu and Luo (2009) and Chen et al. (2017b).

When calculating the optical parameters of aerosols, the scheme by Yu et al. (2012) was used. The particles are assumed to be spherical and key particle optical properties including extinction efficiency, single scattering albedo (SSA), and asymmetry parameter at each wavelength are calculated by Mie theory based on the core diameter, shell diameter, real and imaginary components of the refractive index of core and shell. The core-shell code based on Toon and Ackerman (1981) is used in APM. To reduce computation cost, three lookup tables are used: one for particles without solid absorbing cores, the second for coated BC, and the third for coated dust. The volume-averaged refractive indices of species other than BC and dust are calculated based on the composition simulated by NAQPMS. Details can be seen in Yu et al. (2012) and references therein.

2.3 Sensitivity test design

In this study, the 3-D chemical transport model NAQPMS coupled with the advanced particle microphysics module (APM) was used to reproduce the evolution and spatial distribution of pollutants. The mass concentration, size distribution, and mixing state of aerosols are calculated by NAQPMS+APM. FlexAOD is a module that calculates the extinction property of aerosols under different mixing state assumptions based on Mie theory and a fixed size distribution, using the input of aerosol components' mass concentration and relative humidity as shown in **Sect. 2.2.1**. There are two approaches to calculating optical properties. The absorption property of aerosols can be investigated by FlexAOD with the input of component concentration simulated by NAQPMS+APM and assumed size distribution. The fraction of embedded BC and the fraction of coating aerosols calculated by NAQPMS+APM can be used to constrain the mixing state in FlexAOD. In the other approach, the absorption property can be investigated by the optical module based on APM with core and shell information calculated by NAQPMS+APM as shown in **Sect. 2.2.2**. Then a series of sensitivity tests were designed to explore the impact of mixing state, components, aging process, and detailed microphysical processes (Table 1).

Firstly, to examine the effect of mass concentration and mixing state on the optical properties, sensitivity tests with different mixing states (external, internally homogeneous, and core-shell) were conducted using FlexAOD. EXTo, HOMo, and CSo refer to cases calculated using FlexAOD with observed components as input under external, homogeneous internal,

and core-shell mixing states, respectively. EXTs, HOMs, and CSs refer to cases calculated using FlexAOD with components simulated by NAQPMS+APM as input under external, homogeneous internal, and core-shell mixing states, respectively. Comparing EXTo, HOMo, and CSo can reveal the impact of the mixing state, and similarly, comparing EXTs, HOMs, and CSs further demonstrates this impact. Comparing CS_O with CS_S, the impact of mass concentration on optical properties can be obtained. Secondly, to investigate the impact of the aging process, simulations were designed using a partial core-shell mixing state in FlexAOD, encompassing two scenarios: CS-F_{in} (all secondary aerosols coating the F_{in} fraction of embedded BC, where "fraction" refers to mass fraction throughout this study) and CS-$F_{in}F_c$ (F_c fraction of secondary aerosols coating the F_{in} mass fraction of embedded BC), as illustrated in Fig. S2. Additionally, components, size distribution, and mixing state simulated by NAQPMS+APM were used to calculate the optical properties (CS-APM). The impact of the microphysical process can be investigated by comparing CS-$F_{in}F_c$ with CS-APM.

Table 1 Simulation test design

Case	Method	Input	Size distribution	Mixing state
EXT$_O$	FlexAOD	observed	fixed	external
HOM$_O$	FlexAOD	observed	fixed	internal homogeneous
CS$_O$	FlexAOD	observed	fixed	core-shell
EXT$_S$	FlexAOD	simulated	fixed	external
HOM$_S$	FlexAOD	simulated	fixed	internal homogeneous
CS$_S$	FlexAOD	simulated	fixed	core-shell
CS-F_{in}	FlexAOD	simulated	fixed	partial core-shell and partial bare BC [a]
CS-$F_{in}F_c$	FlexAOD	simulated	fixed	partial core-shell, partial bare BC, and partial coating aerosols [b]
CS-APM	APM	simulated	simulated	semi-external (hourly) [c]

Impact	Description
EXT$_O$ vs. HOMo vs. CSo	Impact of mixing state when inputting observed data
EXT$_S$ vs. HOM$_S$ vs. CS$_S$	Impact of mixing state when inputting simulated data
CSo vs. CSs	Impact of aerosol mass concentration
CSs vs. CS-F_{in}	Impact of aging process (fraction of embedded BC)
CSs vs. CS-$F_{in}F_c$	Impact of the aging process (fraction of embedded BC and coating shell)

205 [a] Aerosols are classified into two types: embedded, bare-like BC aerosols.

[b] Aerosols are classified into three types: embedded, bare-like BC, and BC-free aerosols.

[c] The concept map can be found in Chen et al. (2019, Figure 1).

2.4 Model evaluation

Statistical parameters such as the correlation coefficient (R), normalized mean bias (NMB), index of agreement (IOA), the
210 fraction of the simulations within a factor of two of the observations (FAC2), mean fractional bias (MFB) and mean
fractional error (MFE) were used in this study to evaluate the performance of NAQPMS (Table S3). NAQPMS reproduced
the temporal distribution of PM$_{2.5}$ in Beijing well (Fig. 2). As shown in Table S4, the R between the observed and simulated
hourly PM$_{2.5}$ concentrations of six sites over Beijing-Tianjin-Hebei and surrounding regions were within 0.55~0.76. The
NMB was within -0.22~0.13, which satisfied the model performance criteria proposed by Emery et al. (2016). There was
215 only a small overestimation of 13% in the simulated PM$_{2.5}$ in Zhengzhou. And the IOA reached more than 0.72. The MFB
and MFE of PM$_{2.5}$ in all six sites were within the benchmarks, which satisfied the model performance criteria proposed by
Boylan and Russell (2006).
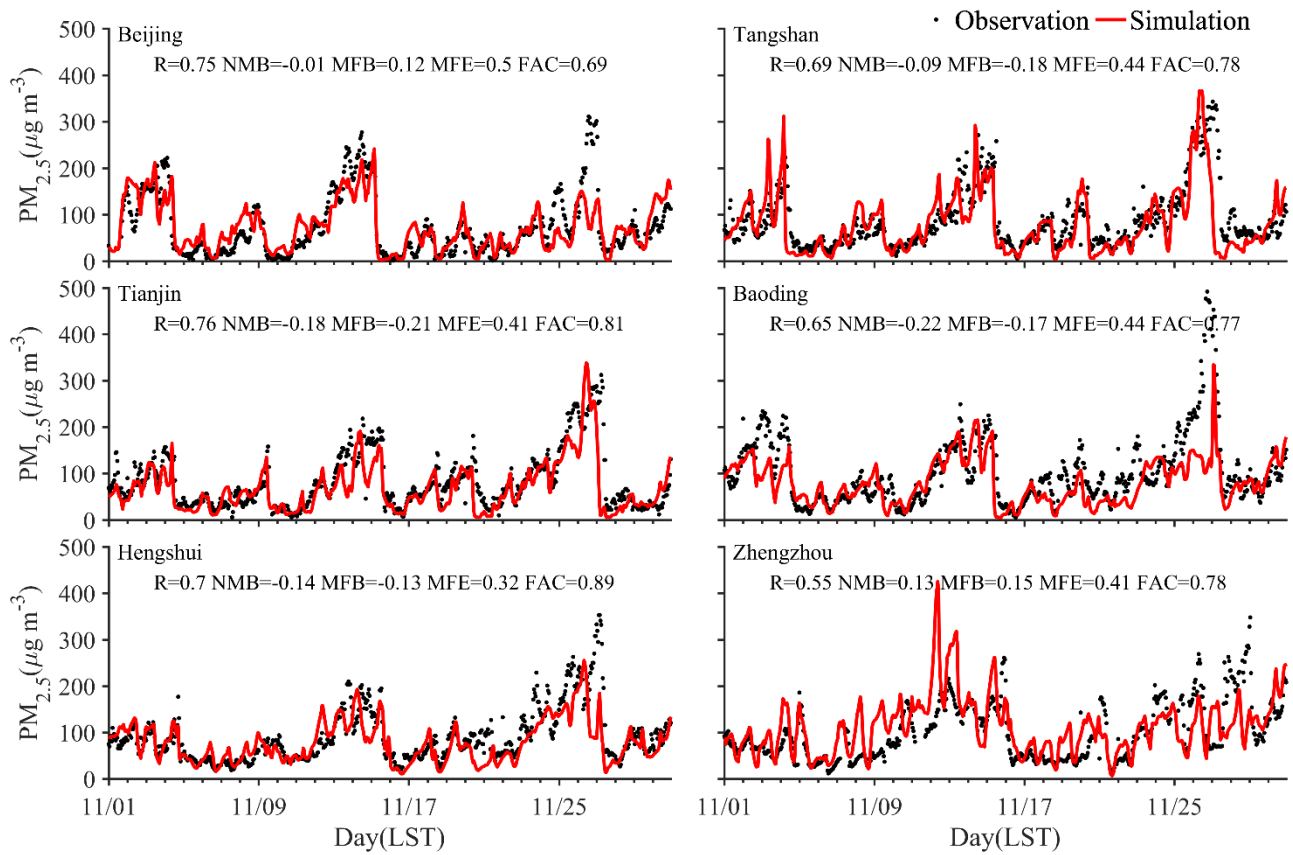
Figure 2. Model evaluation of PM$_{2.5}$ at six sites in the Beijing-Tianjin-Hebei region in November 2018.

NAQPMS also exhibited good performance in representing the PM$_{2.5}$ components in Beijing (Fig. 3). The R values between the observed and simulated nitrate, sulfate, ammonium, element carbon, primary organic aerosols, and secondary organic aerosols were 0.74, 0.83, 0.74, 0.55, 0.48, and 0.23 in Beijing, respectively. However, the simulation of secondary inorganic aerosols was underestimated by -62%~-8%. This is likely caused by insufficient heterogeneous formation of sulfate and nitrate (Li et al., 2018). Black carbon and primary organic aerosols were overestimated by 7.2% and 11.5%, which is probably related to the emission inventory. Monthly mean emissions were used in this study and there is substantial uncertainty in emission inventory (Li et al., 2017). However, the reasonable simulation of aerosol mass concentration lays a solid foundation for simulating the optical properties of BC-containing aerosols.
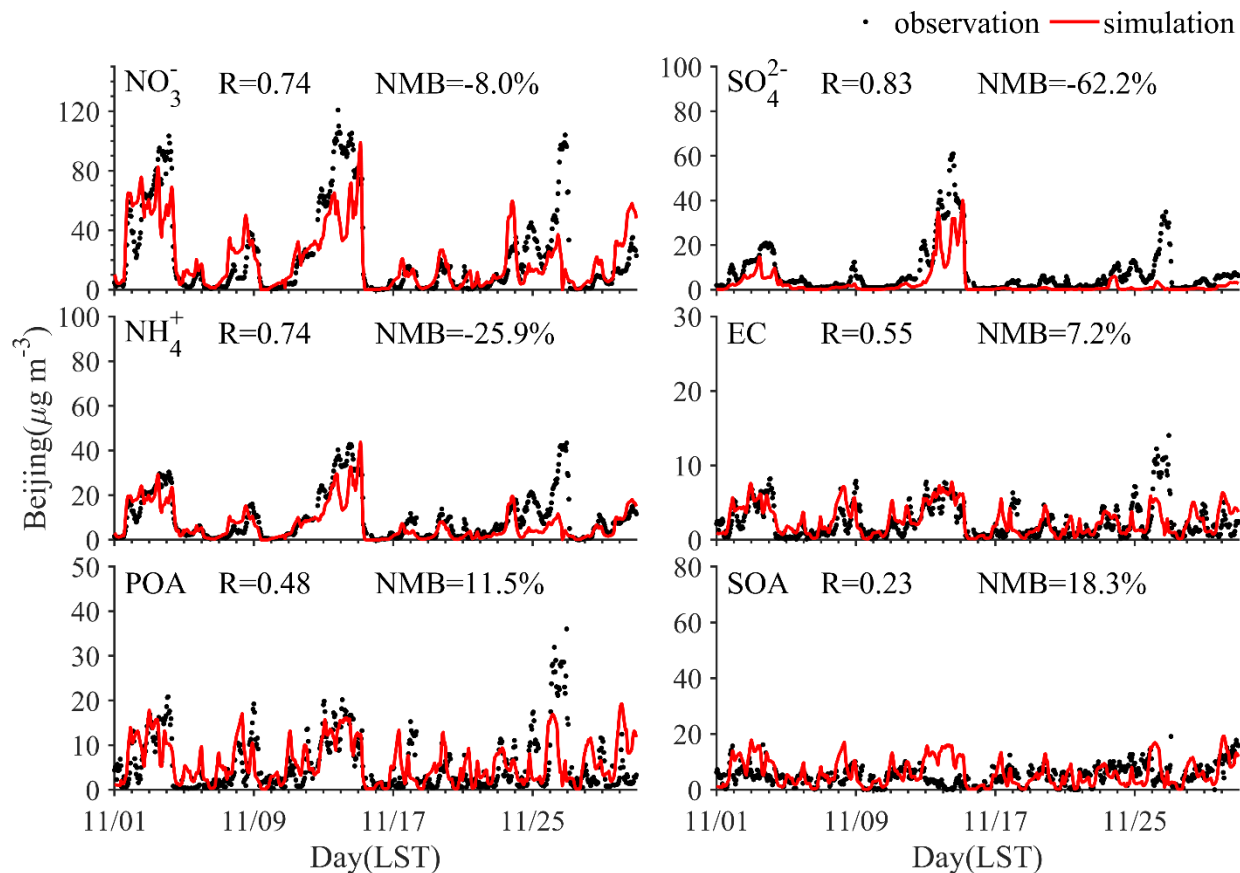
Figure 3. Simulated and observed PM$_{2.5}$ components in Beijing

3 Results

3.1 Absorption properties based on observed components

3.1.1 Description of observations

The time series and proportion of various chemical components of PM$_{2.5}$ are shown in Fig. 4. During the study period, the average mass concentration of PM$_{2.5}$ was 74.4 ± 68.7 μg m^{-3}. Nitrate is the main component of PM$_{2.5}$, accounting for 36.4% on average, followed by organic matter, ammonium, and sulfate, accounting for 16.6%, 15.4% and 11.5%, respectively. EC, crustal elements, and chloride salt accounted for 3.9%, 8.8%, and 4.1%, respectively. The average RH during the period was 39 ± 17.9% and the temperature was 8.3 ± 3.2 °C. The average b_{sca} (±1σ) and b_{abs} (±1σ) at 630 nm during the study period were 169.1 ± 212.3 Mm^{-1} and 46.5 ± 48.5 Mm^{-1} in Beijing, respectively. The average b_{abs} (±1σ) at 880 nm during the study period were 30.7 ± 25.2 Mm^{-1}. The b_{abs} at 880 nm and EC mass concentration are highly correlated (Fig. S3). The decrease in visibility is mainly caused by particle scattering extinction. The b_{sca} and b_{abs} in this study were much lower than those

observed in Beijing in the winter of 2016 (Xie et al., 2019), but the b_{ext} in this study was higher than that observed in Beijing in the winter of 2019 (Sun et al., 2021), indicating that the decreases in PM$_{2.5}$ in recent years also caused similar reductions in extinction coefficients.
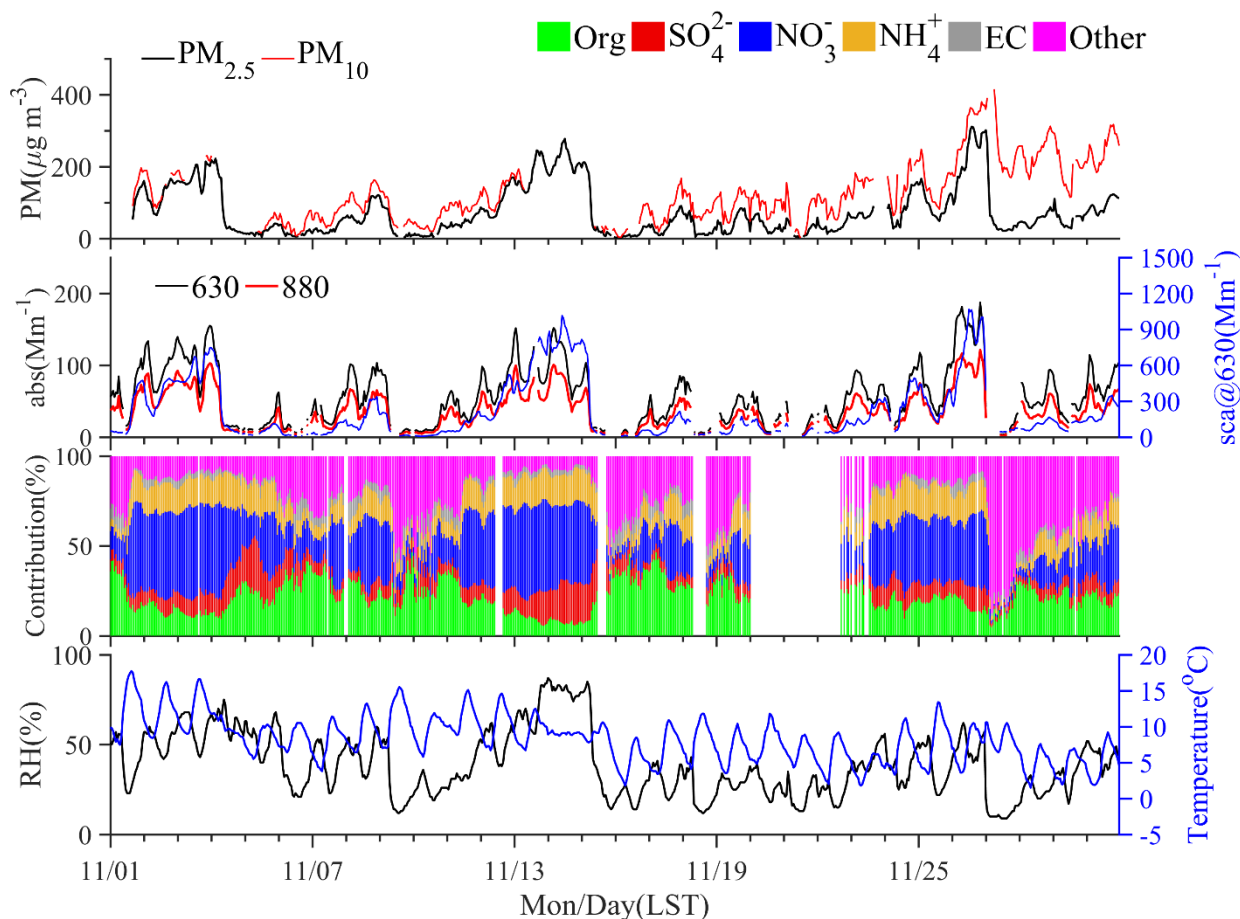
Figure 4. Evolution of observed PM$_{2.5}$, components, aerosol extinction coefficient, and meteorology parameters in November 2018 at Beijing

3.1.2 Absorption coefficient calculated by FlexAOD based on observation

The observed PM$_{2.5}$ components and RH were used to calculate the optical properties using FlexAOD. It should be noted that the times missing component data were excluded when calculating optical properties. Comparison between the observed and simulated absorption coefficients shows that the simulations by FlexAOD under the three mixing state assumptions are highly correlated with the observations, and the correlation coefficient can reach 0.88, demonstrating the usability of the FlexAOD model in Beijing. However, using different mixing state assumptions led to widely varying results, see Figure 5. On average, the b_{abs} at 880 nm calculated for the core-shell mixing state was 2.4 times higher than that for external mixing. For the external mixing state, the calculation was underestimated by 59%, while it was overestimated by 91% under uniform

internal mixing. The simulation for core-shell mixing was closest to observations, with an underestimation of 2.8%. The absorption coefficient under uniform internal mixing is the highest, followed by core-shell mixing and the calculation for external mixing is the lowest. This is consistent with the findings of Curici et al. (2019). The assumption of either internal mixing or external mixing alone is not realistic, and partial internal mixing with partial coating closely approximates reality and should be considered for absorption calculations as reported by Curci et al. (2019).
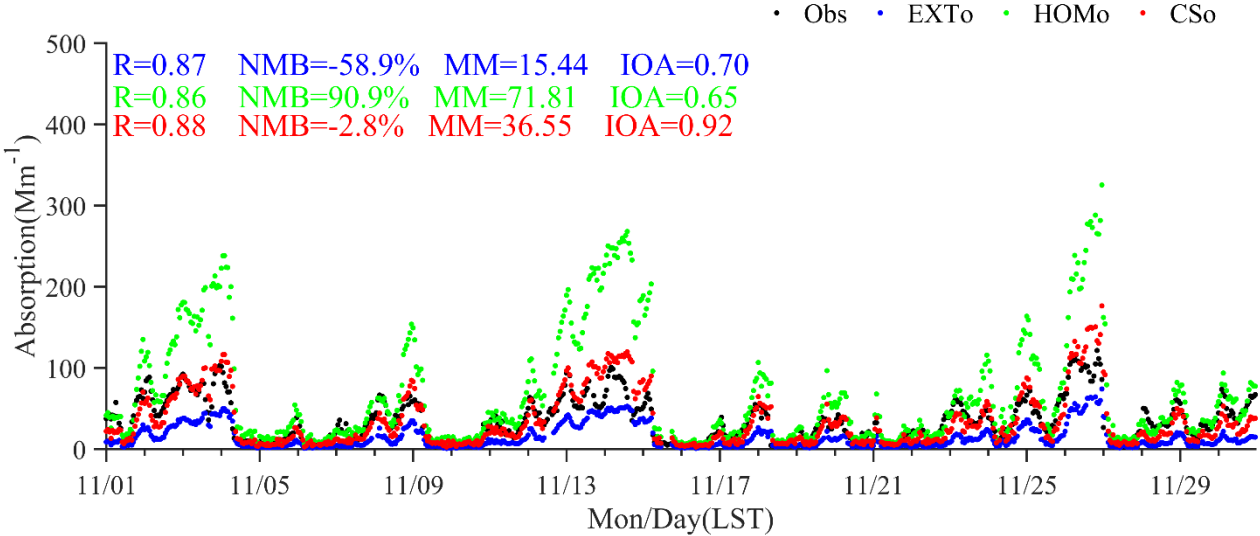
Figure 5. Observed and calculated absorption coefficients at 880 nm under external mixing (EXTo), homogeneous internal mixing (HOMo), and core-shell mixing (CSo) by FlexAOD based on observed components.

3.2 Absorption property based on simulations by NAQPMS

A comparison of the absorption coefficients between observation and calculation with FlexAOD based on $PM_{2.5}$ simulations from NAQPMS with different mixing states can be seen in Table 2. In this study, only times in which the simulated $PM_{2.5}$ was within a factor of two of the observations were considered in the optical calculation. The average of observed b_{abs} is 43 Mm^{-1}. There were large variations in the absorption coefficient under different mixing states. In the EXTs case, the absorption coefficient at 880 nm was underestimated by 54%, and only 40% of the modeled values were within a factor of 2 of the observations. In the HOMs case, the absorption at 880 nm was largely overestimated by 95%, with 58% of the modeled values falling within a factor of two of the observations. In the CS_S case, FAC2 increased to 0.93 compared with EXTs simulations, and the model overestimated the absorption coefficient by 10%. Among the three ideal mixing state assumptions in this study, the result of the core-shell mixing state assumption is closest to the observed absorption coefficient. It should be noted that there are uncertainties associated with the calculation. As shown in Figure 3, the concentration of secondary inorganic aerosols is underestimated by the NAQPMS model while BC is overestimated; consequently, the coated thickness may be underestimated. Comparing the results of CS_S with CS_O (where calculations with

FlexAOD were based on observed components under a core-shell mixing state), the results show that the effect of simulated components on the absorption coefficient can be up to 13%, which is much smaller than the impact of the mixing state.
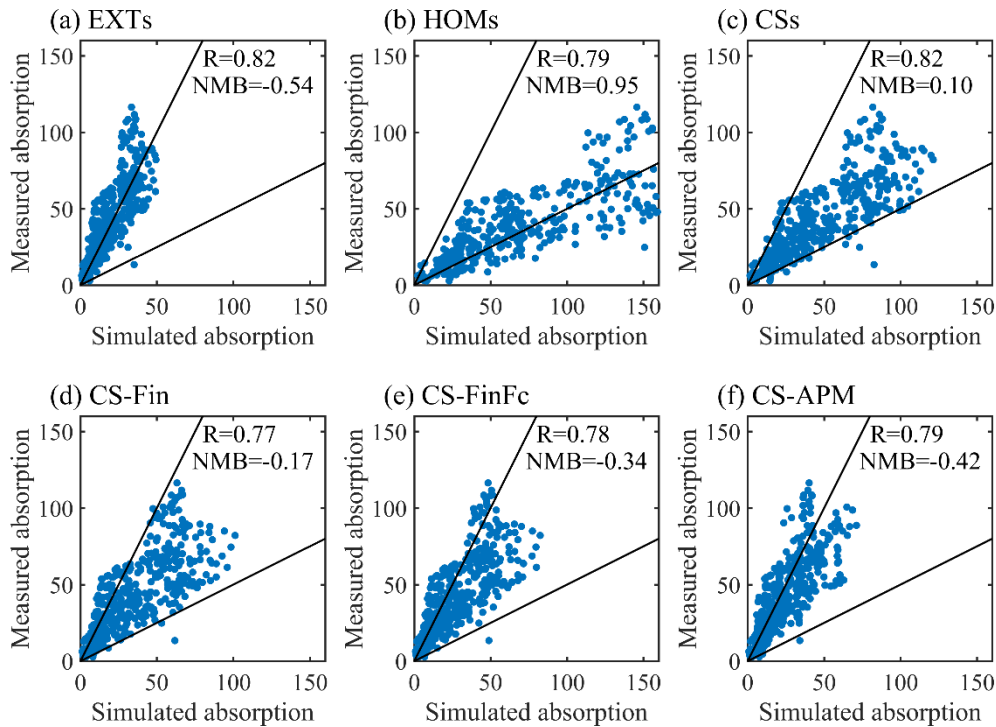
Figure 6. Comparison of observed and simulated absorption coefficients at 880 nm under different mixing states (EXT$_S$, HOM$_S$, CS$_S$, CS-F$_{in}$, CS-F$_{in}$F$_c$, and CS-APM) at the IAP in Beijing.

Table 2. Intercomparison of the performance of absorption coefficients at 880 nm under different mixing states. b is the ratio of simulation to observation.

Schemes	b	R	NMB	FAC2
EXT$_S$	0.46	0.82	-0.54	0.40
HOM$_S$	1.95	0.79	0.95	0.58
CS$_S$	1.10	0.82	0.10	0.93
CS-F$_{in}$	0.83	0.77	-0.17	0.84
CS-F$_{in}$F$_c$	0.66	0.78	-0.34	0.66

| CS-APM | 0.58 | 0.79 | -0.42 | 0.72 |

3.3 Constraint of the fraction of embedded BC and secondary components coating aerosols

In the real world, the mixing state of particles is complex. Wang et al. (2021b) found using an electron microscope that the
embedded fraction of BC significantly influenced the absorption. In the extremely polluted winter period of January 2013,
more than half of BC particles were thickly coated by non-refractory materials (Wu et al., 2016). Along with the
implementation of the Air Pollution Prevention and Control Action Plan, the mass of BC and the fraction of thickly coated
BC changed (Wu et al., 2021). Cheng et al. (2012) proposed that the fraction of internally mixed particles can be
parameterized based on oxidized nitrogen oxides and total reactive nitrogen. Curci et al. (2019) used the mass ratio of
secondary inorganic aerosols and organics to BC as the fraction of internally mixed particles.

Emitted hydrophobic black carbon becomes hydrophilic due to aging processes. In this study, the aging of BC can be
resolved by NAQPMS+APM. The detailed aging processes of aerosols are considered in a physical manner. The model
represents the aging processes by simulating condensation and coagulation. The ratio of hydrophilic BC to total BC is used
as a proxy for the fraction of embedded BC. The evolution of the ratio of particle diameter to BC-core size (Dp/Dc), the
fraction of embedded BC (F_{in}), and the fraction of secondary components coating on BC (F_c) at the site in Beijing is shown
in Fig. 7. When F_{in} is equal to 0, it means the BC is externally mixed with other aerosols, and when F_{in} is equal to 1, it means
all BC particles are coated by other aerosols. The average ratio of F_{in} during the study period in Beijing is 34.1%, which is a
bit lower than the ratio of 0.48 and 0.63 obtained by the method of Cheng et al. (2012) and Curci et al. (2019), respectively.
Also, F_{in} in this study is closely related to the ratio of secondary inorganic aerosols to BC, with an R of 0.72. Zheng et al.
(2022) also found that secondary inorganic aerosols dominated the light absorption enhancement with online observational
datasets. We consider a separate case, CS-F_{in}, where the F_{in} mass fraction of BC particles is core-shell mixed with other
aerosols, and a 1-F_{in} fraction of BC particles is bare and external mixing. The calculated absorption at 880 nm (b_{abs_880}) for
the CS-F_{in} case was 35.5 Mm^{-1}, which was close to the measured mean value, and 84% of simulations of absorption
coefficients were within a factor of two of the observations.
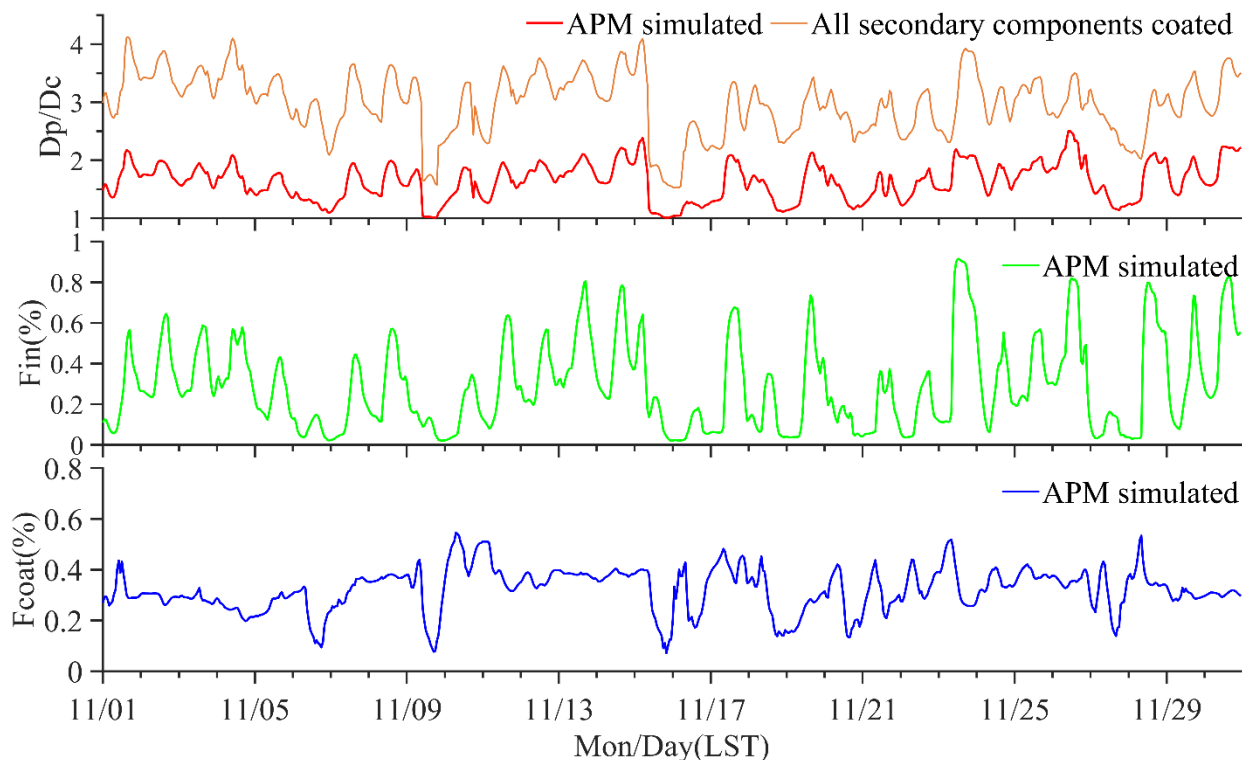
Figure 7. Evolution of ratio of particle diameter to BC-core size (Dp/Dc), the fraction of embedded BC (Fin), and the fraction of secondary components coating on BC (Fc) at IAP in Beijing. "APM simulated" refers to parameters simulated by the advanced particle microphysics module in NAQPMS.

Aerosols in the atmosphere include BC-containing aerosols (coated BC and bare BC) and BC-free aerosols (Zhao et al., 2022). In this study, the fraction of secondary aerosol coating on BC is also considered in the optical calculation. As sulfate aerosols include sulfate coating on BC, OC, dust, and sea salts, then the fraction of sulfate coating on BC was used as the fraction of secondary components coating on BC (F_c). When F_c is equal to 0, there is no coating on BC particles, and when F_c is equal to 1, it means all other aerosols are coated on BC. We thus consider a scenario CS-$F_{in}F_c$, where the F_{in} fraction of BC particles and the F_c fraction of secondary components are core-shell mixed, and other aerosols are externally mixed. The average F_c during the study period in Beijing is 34.3%. The calculated absorption at 880 nm for the CS-$F_{in}F_c$ case was 28.1 Mm^{-1}, and 66% of the simulations of absorption coefficients were within a factor of two of the observations.

As described in **section 2.2.2**, the optical properties were calculated based on Mie theory using the core and shell information derived from APM considering microphysical processes. The observed absorption coefficient and that simulated by NAQPMS+APM under a semi-external mixing state, namely CS-APM, is shown in Table 2 and Fig. 6f. The results show that the simulated absorption at 880 nm matches the observation reasonably well, with an R of 0.79, although there is an underestimation with NMB of 0.42. The CS-$F_{in}F_c$ case considers the fraction of embedded BC and the fraction of secondary components coating BC calculated with APM. Comparison between CS-$F_{in}F_c$ and CS-APM reveals the impact of accounting

for the detailed microphysical process on absorption property. The FAC2 of 0.72 in the CS-APM case is greater than 0.66 in the CS-$F_{in}F_c$ case. The underestimation of 42% in CS-APM is larger than the 34% in CS-$F_{in}F_c$. This underestimation can be attributed to the assumed morphology of BC-containing particles, the size distribution of primary particles input to APM, and the concentration of secondary components coated on BC. As shown in Fig. 3, there is an underestimation of 8-62% in the simulation of secondary inorganic aerosols. Even if the model accurately captures the physical processes of aerosols, the coating on BC could be underestimated because of the representation uncertainties in chemical formation, potentially impacting the accuracy of the absorption calculation.

3.4 Light absorption enhancement due to mixing state and aging processes

The light absorption enhancement is the ratio of the light absorption coefficient of coated BC and bare BC. E_{abs} is proposed to quantify the lensing effects, however, large uncertainty exists in E_{abs} and the radiative effect of black carbon. In this study, the BC absorption enhancement is calculated as the ratio of the absorption coefficient calculated assuming core-shell mixing (including CSs, CS-F_{in}, and CS-$F_{in}F_c$ cases) to that calculated using external mixing.

$$E_{abs} = \frac{b_{abs}(\lambda, core - shell\ mixing)}{b_{abs}(\lambda, external\ mixing)}$$

3.4.1 The impact of the detailed microphysical process on absorption enhancement

We modified the APM module in NAQPMS so that BC does not mix with other chemical species in the calculation of the microphysical process and optical properties. This sensitivity test was conducted by turning off the coating process in APM. The radiative absorption enhancement in the CS-APM case was the ratio of the absorption coefficient in the base simulation to that in the sensitivity test.

The mass ratio of the coating of BC to BC (MR) can be used to represent the aging degree (Du et al., 2019; Wang et al., 2019). To compare with previous studies, E_{abs} values at 630 nm are shown in Fig. 8. The evolution of E_{abs} and MR shows that E_{abs} is positively correlated to MR, and the R can reach 0.88. This is consistent with Liu et al. (2017) who showed that E_{abs} is closely related to MR. Under the same MR, E_{abs} can vary by 0.49. When MR equals 3, E_{abs} varied by 0.25. The E_{abs} in the CS-APM case in Beijing is much higher than the measurements in Taizhou (Zhao et al. 2021). However, the measurements in Beijing by Xie et al. (2019) fall in the range of this study when MR is less than 5. E_{abs} in the CS-APM case is higher than that from the laboratory study in Peng et al (2016) when MR is less than 3, but it is lower when MR exceeds 5.

The spatial distribution of E_{abs} at 880 nm (E_{abs_880}) is shown in Fig. 9d. The E_{abs_880} over Beijing-Tianjin-Hebei and the surrounding region was about 1.3~1.8. The E_{abs_880} in the CS-APM case is a bit higher than that in the CS-$F_{in}F_c$ case. The spatial distribution of E_{abs_880} also showed lower values of 1.3~1.7 over the source region and higher values of 1.6~1.8 over the outflow region. The average E_{abs} at Beijing at 630 nm and 880 nm from APM and Mie theory are 1.58 and 1.55.
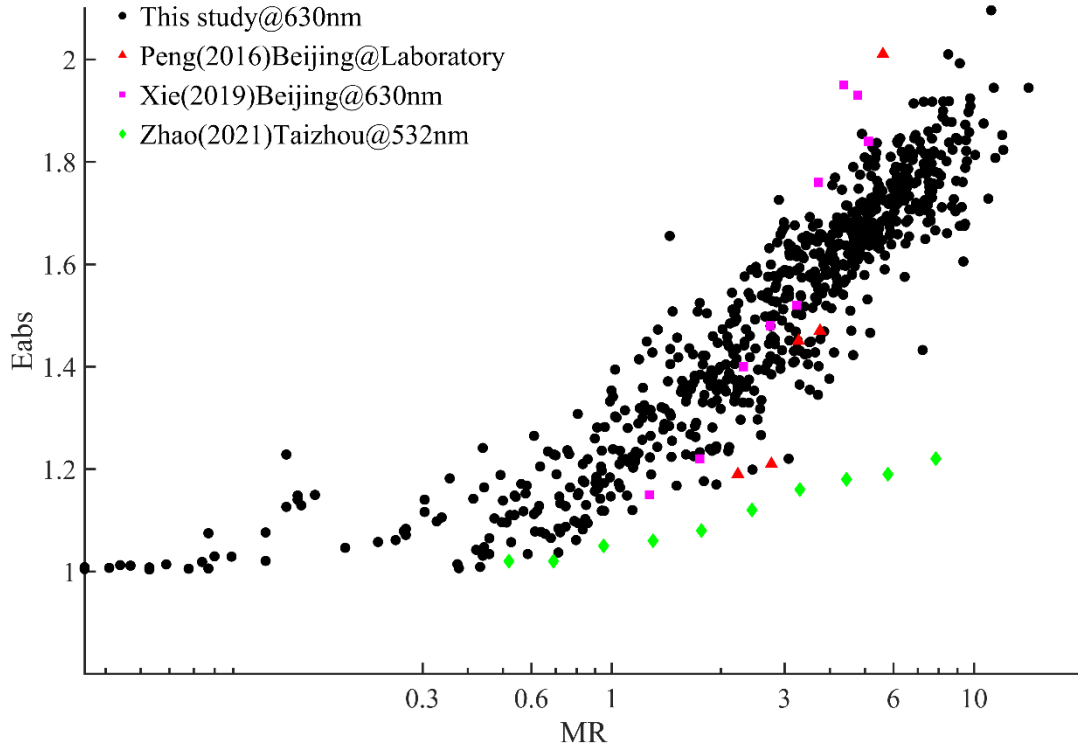
Figure 8. The absorption enhancement in the CS-APM case under different mass ratios (MR) of coating materials and BC core

3.4.2 Impact of the aging processes on light absorption enhancement

The spatial distribution of E_{abs} at 880 nm is shown in Fig. 9. The spatial distribution of the absorption enhancement in CS-F_{in} and CS-$F_{in}F_c$ cases shows that E_{abs} is lower near the emission source and higher in the outflow region (Bohai and Yellow Sea, Taihang mountain). This is because BC has aged by condensation and coagulation processes during transport in the atmosphere. As shown, the values of E_{abs_880} over Beijing-Tianjin-Hebei and the surrounding region from FlexAOD under the core-shell mixing state are about 2.0~2.5. After considering the fraction of embedded BC, the E_{abs} decreased to 1.3~2.1, representing a decrease of 11%~34%. Considering the fraction of embedded BC and the fraction of coating, the E_{abs} decreased to 1.2~1.7, representing a decrease of 30%~43%. The values of E_{abs} in the CS-$F_{in}F_c$ case are 1.2~1.5 near the emission sources and 1.5~1.7 over the outflow region. These values are similar to the currently accepted range of 1.2–1.6 (Bond et al., 2013; Matsui et al., 2016; Liu et al., 2017; Curci et al., 2019). The distribution of average E_{abs} and SSA values with height in Beijing is shown in Fig. 10. E_{abs} increased with height while SSA decreased with height in CS-F_{in} and CS-$F_{in}F_c$ cases. Relatively low E_{abs} values (1.3~1.6) are concentrated in layers below 500 m. This is related to the low level of anthropogenic emissions and to the ability of BC in the upper layer to be transported over wider regions.
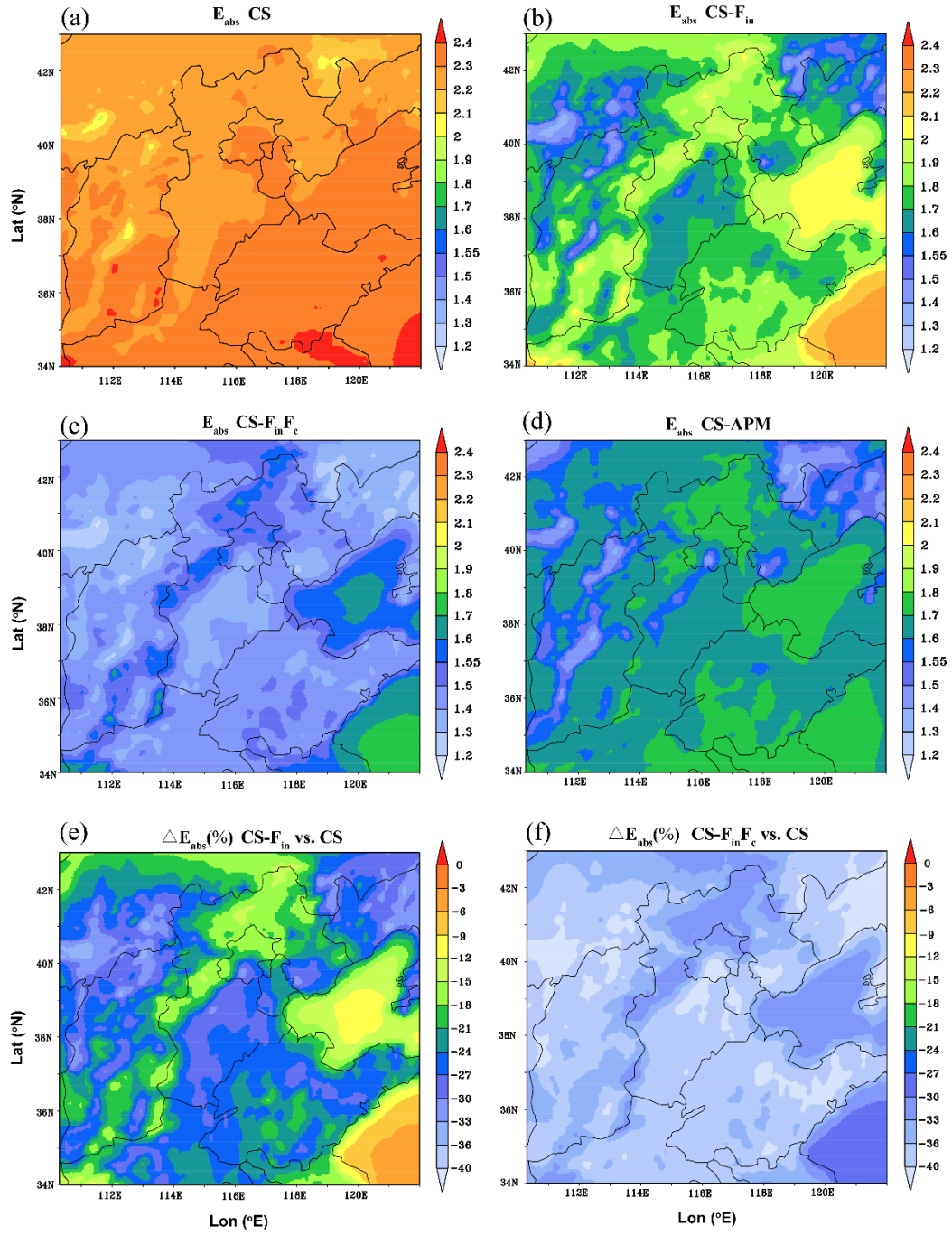
Figure 9. The absorption enhancement at 880 nm in (a) core-shell mixing (CS), (b) CS-F_{in}, (c) CS-$F_{in}F_c$, and (d) CS-APM cases. And changes in radiation absorption enhancement in (e) CS-F_{in} and (f) CS-$F_{in}F_c$ cases compared with core-shell mixing.
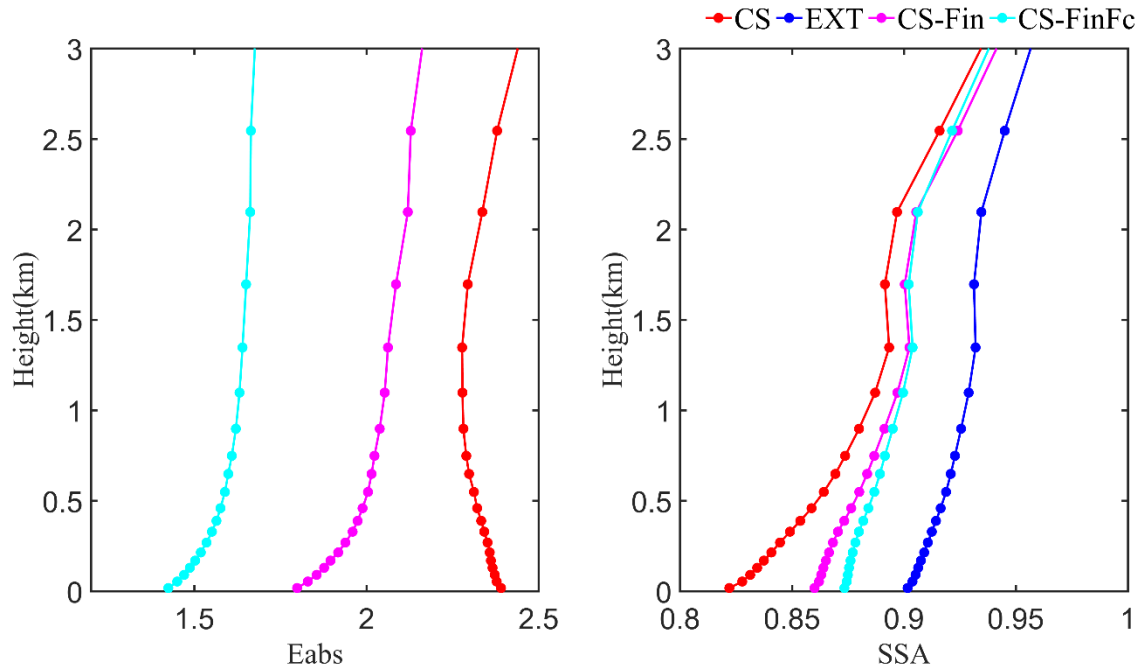
Figure 10. The distribution of E$_{abs}$ and SSA values with height

In Beijing, the absorption enhancement at 630 nm and 880 nm is 2.65 and 2.39 for the core-shell mixing state using FlexAOD (Fig. 11). When considering the fraction of embedded BC, the E$_{abs}$ values in the CS-F$_{in}$ case at 630 nm and 880 nm are 1.94 and 1.80, decreasing by 26.7% and 24.5% compared to the CS case, respectively. If the fraction of secondary aerosol coating on BC is also considered at the same time, the E$_{abs}$ values in the CS-F$_{in}$F$_c$ case at 630 nm and 880 nm are 1.51 and 1.43, decreasing by 43% and 40.2% compared to the CS case, respectively. Therefore, considering the fraction of secondary aerosol coating on BC, E$_{abs}$ at 630 nm and 880 nm can decrease by 16.2% and 15.7%, respectively, compared to the CS case. The ratios of E$_{abs}$ at 880 to E$_{abs}$ at 630 nm under different mixing states in this study were consistently less than 1. This is consistent with the fact that E$_{abs}$ are expected to decrease with increasing wavelength (Liu et al., 2018).

380
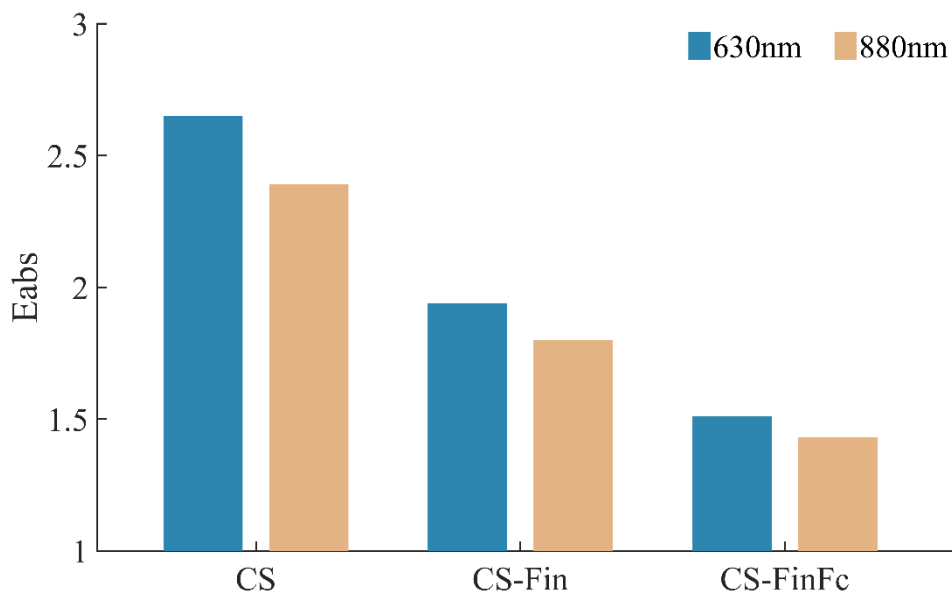
Figure 11. The radiation absorption enhancement at 630 nm and 880 nm under different mixing state assumptions in Beijing.

Comparing the E_{abs} obtained in this study under different mixing states with previous studies, the E_{abs} in CS-F_{in} and CS-$F_{in}F_c$ cases considering the aging process were a bit higher than other laboratory and ambient measurement studies in Beijing (1.03~1.3) (Wang et al., 2019). Sun et al. (2021) using the thermodenuder (TD) method found that E_{abs} at 870 nm at an urban

385 site in Beijing was 1.24 ± 0.15. Zhang et al. (2021) using the mass absorption cross section (MAC) method by SP2 found that E_{abs} at 880 nm at a rural site in Gucheng was 1.33 ± 0.57. Cui et al. (2016) found that the E_{abs} increased from 1.4 during fresh combustion to approximately 3 for aged BC at a rural site on the North China Plain. But the results for CS-F_{in}, CS-$F_{in}F_c$, and CS-APM cases were lower than those in other model simulations (Curci et al., 2019; Tuccella et al., 2020). The results show that accounting for the aging process of BC has a significant effect on the absorption enhancement, and should be

390 considered during model E_{abs} calculation.

4 Conclusions and discussion

Black carbon-containing aerosols have a significant impact on global warming. However, the extent of the impacts is highly uncertain. Component concentration, mixing state, and aging processes are important parameters. In this study, observed and simulated concentrations of $PM_{2.5}$ components in November 2018 are used with Mie theory to investigate the impact of the

395 mixing state and aging process on the light absorption properties of aerosols.

Through a series of sensitivity tests, a systematic comparison was conducted to explore the impacts of components, mixing state, aging process, and detailed microphysics on absorption properties. Under the same mixing state with observed

and simulated components, b_{abs} can be highly impacted by the simulated concentration of PM$_{2.5}$ components. Sensitivity tests with different mixing states (external, internally homogeneous, and core-shell) using FlexAOD showed that different mixing state assumptions led to widely varying results. The absorption coefficient is highest under uniform internal mixing, lower under core-shell mixing, which is closest to observation, and lowest under external mixing.

Considering the fraction of embedded BC and secondary components coating on BC is a compromise and reasonable solution to represent the mixing state of BC in a three-dimensional model although uncertainties exist. The detailed microphysical processes can be resolved by an advanced particle microphysics module in NAQPMS. The ratio of hydrophilic BC and total BC is used as a proxy for the fraction of embedded BC and the fraction of sulfate coating on BC is used as a proxy for the fraction of secondary components coating BC. Then the fraction of embedded BC and secondary components coating aerosols was used to constrain the mixing state. The simulation of absorption is also reasonable when considering the fraction of embedded BC and coating of secondary components on BC, as this reflects a more realistic mixing state. The NMB of the simulated absorption coefficient has changed from 10% to -34% in Beijing, and the R changed from 0.82 to 0.78.

Accounting for the aging process of BC has a significant effect on radiative absorption enhancement. The E$_{abs}$ at 880 nm over the Beijing-Tianjin-Hebei area reduced from 2.0~2.5 under core-shell mixing state to 1.3~2.1 when considering the fraction of embedded BC, and to 1.2~1.7, a decrease of 30%~42%, when considering the fraction of embedded BC and the fraction of coating. Considering the detailed microphysical processes, E$_{abs}$ in the CS-APM case was positively correlated with MR with an R of 0.88. The E$_{abs}$ values in CS-F$_{in}$F$_c$ and CS-APM cases were a bit higher than those from other laboratory and ambient measurement studies in Beijing but were within the range of previous studies.

The optical properties can be affected by uncertainties in the size distribution of primary particle emissions (Zhou et al. 2012; Matsui, 2016). Geometric radius and standard variation are two important parameters of size distribution. The optical depth of mineral dust and organic was sensitive to standard variation (Obiso and Jorba, 2018). There is a sectoral and spatial difference in the size distribution of primary emissions (Paasonen et al., 2016). Sensitivity tests should be conducted to see the impact of size distribution on σ_{abs} and E$_{abs}$ in future studies. More efforts considering the morphology and the absorption characteristics of coating can also help understand the radiative effect of BC-containing aerosols (Liu et al., 2020; Li et al., 2024).

Overall, this study underscores the importance of representing microphysical processes related to BC aerosols and their mixing state. Our results indicate that resolving the fraction of coated BC and the coating layer can significantly impact the calculated E$_{abs}$. Although modeling the mixing state and microphysical processes is challenging for the chemical transport model, the fraction of aged BC and coating aerosols can be used to constrain the mixing state. This study provides a reference for simulating the radiative effect of black carbon aerosols using three-dimensional models.

Data availability.

The PM$_{2.5}$ observation data can be obtained from the China National Environmental Monitoring Centre (https://air.cnemc.cn:18007/). The simulated data of this study are available upon request to the corresponding author.

Author contributions.

HD, JL and XC designed the work. HD performed the simulation and analysis. Gabriele C and ZFW provided the software. YS, XD and SG processed the measurement data. ZW, WY and LW validated the simulated data. HD wrote the original draft with assistance from co-authors. JL, XC and FY reviewed and edited the manuscript.

Competing Interests

At least one of the (co-)authors is a member of the editorial board of Atmospheric Chemistry and Physics.

Acknowledgements

We thank the support of the Technological Infrastructure project "Earth System Science Numerical Simulator Facility" (EarthLab). The FlexAOD code can be provided upon request to gabriele.curci@aquila.infn.it.

Financial support.

This research was supported by the Strategic Priority Research Program (B) of the Chinese Academy of Sciences (XDB0760302), the National Key R&D Program of the Ministry of Science and Technology, China (grant no. 2022YFC3700703), the National Natural Science Foundation of China (NSFC) research project (42207133, 42377105).

References

Bond, T. C., Doherty, S. J., Fahey, D. W., Forster, P. M., Berntsen, T., DeAngelo, B. J., Flanner, M. G., Ghan, S., Karcher, B., Koch, D., Kinne, S., Kondo, Y., Quinn, P. K., Sarofim, M. C., Schultz, M. G., Schulz, M., Venkataraman, C., Zhang, H., Zhang, S., Bellouin, N., Guttikunda, S. K., Hopke, P. K., Jacobson, M. Z., Kaiser, J. W., Klimont, Z., Lohmann, U., Schwarz, J. P., Shindell, D., Storelvmo, T., Warren, S. G., and Zender, C. S.: Bounding the role of black carbon in the climate system: A scientific assessment, Journal of Geophysical Research-Atmospheres, 118, 5380-5552, 10.1002/jgrd.50171, 2013.

Bondy, A., Bonanno, D., Moffet, R., Wang, B., Laskin, A., and Ault, A.: The diverse chemical mixing state of aerosol particles in the southeastern United States, Atmospheric Chemistry and Physics, 18, 12595-12612, 10.5194/acp-18-12595-2018, 2018.

Boylan, J. W., and Russell, A. G.: PM and light extinction model performance metrics, goals, and criteria for three-dimensional air quality models, Atmospheric Environment, 40, 4946-4959, 10.1016/j.atmosenv.2005.09.087, 2006.

Castro, L., Pio, C., Harrison, R., and Smith, D.: Carbonaceous Aerosol in Urban and Rural European Atmospheres: Estimation of Secondary Organic Carbon Concentrations, Atmospheric Environment, 33, 2771-2781, 10.1016/s1352-2310(98)00331-8, 1999.

Chen, X., Wang, Z., Li, J., Chen, H., Hu, M., Yang, W., Wang, Z., Ge, B., and Wang, D.: Explaining the spatiotemporal variation of fine particle number concentrations over Beijing and surrounding areas in an air quality model with aerosol microphysics, Environmental pollution, 231, 1302-1313, 10.1016/j.envpol.2017.08.103, 2017a.

Chen, X. S., Wang, Z. F., Li, J., and Yu, F. Q.: Development of a Regional Chemical Transport Model with Size-Resolved Aerosol Microphysics and Its Application on Aerosol Number Concentration Simulation over China, Sola, 10, 83-87, 10.2151/sola.2014-017, 2014.

Chen, X. S., Wang, Z. F., Yu, F. Q., Pan, X. L., Li, J., Ge, B. Z., Wang, Z., Hu, M., Yang, W. Y., and Chen, H. S.: Estimation of atmospheric aging time of black carbon particles in the polluted atmosphere over central-eastern China using microphysical process analysis in regional chemical transport model, Atmospheric Environment, 163, 44-56, 10.1016/j.atmosenv.2017.05.016, 2017b.

Chen, X., Yang, W., Wang, Z., Li, J., Hu, M., An, J., Wu, Q., Wang, Z., Chen, H., Wei, Y., Du, H., and Wang, D.: Improving new particle formation simulation by coupling a volatility-basis set (VBS) organic aerosol module in NAQPMS+APM, Atmospheric Environment, 204, 1-11, 10.1016/j.atmosenv.2019.01.053, 2019.

Chen, X., Ye, C., Wang, Y., Wu, Z., Zhu, T., Zhang, F., Ding, X., Shi, Z., Zheng, Z., and Li, W.: Quantifying evolution of soot mixing state from transboundary transport of biomass burning emissions, iScience, 26, 108125, 10.1016/j.isci.2023.108125, 2023.

Chen, X., Yu, F., Yang, W., Sun, Y., Chen, H., Du, W., Zhao, J., Wei, Y., Wei, L., Du, H., Wang, Z., Wu, Q., Li, J., An, J., and Wang, Z.: Global–regional nested simulation of particle number concentration by combing microphysical processes with an evolving organic aerosol module, Atmos. Chem. Phys., 21, 9343-9366, 10.5194/acp-21-9343-2021, 2021.

Cheng, Y. F., Su, H., Rose, D., Gunthe, S. S., Berghof, M., Wehner, B., Achtert, P., Nowak, A., Takegawa, N., Kondo, Y., Shiraiwa, M., Gong, Y. G., Shao, M., Hu, M., Zhu, T., Zhang, Y. H., Carmichael, G. R., Wiedensohler, A., Andreae, M. O., and Poschl, U.: Size-resolved measurement of the mixing state of soot in the megacity Beijing, China: diurnal cycle, aging and parameterization, Atmospheric Chemistry and Physics, 12, 4477-4491, 10.5194/acp-12-4477-2012, 2012.

Cui, X. J., Wang, X. F., Yang, L. X., Chen, B., Chen, J. M., Andersson, A., and Gustafsson, O.: Radiative absorption enhancement from coatings on black carbon aerosols, Science of the Total Environment, 551, 51-56, 10.1016/j.scitotenv.2016.02.026, 2016.

Curci, G., Hogrefe, C., Bianconi, R., Im, U., Balzarini, A., Baró, R., Brunner, D., Forkel, R., Giordano, L., Hirtl, M., Honzak, L., Jiménez-Guerrero, P., Knote, C., Langer, M., Makar, P. A., Pirovano, G., Pérez, J. L., San José, R., Syrakov, D., Tuccella, P., Werhahn, J., Wolke, R., Žabkar, R., Zhang, J., and Galmarini, S.: Uncertainties of simulated aerosol optical properties induced by assumptions on aerosol physical and chemical properties: An AQMEII-2 perspective, Atmospheric Environment, 115, 541-552, 10.1016/j.atmosenv.2014.09.009, 2015.

Curci, G., Alyuz, U., Baro, R., Bianconi, R., Bieser, J., Christensen, J. H., Colette, A., Farrow, A., Francis, X., Jimenez-Guerrero, P., Im, U., Liu, P., Manders, A., Palacios-Pena, L., Prank, M., Pozzoli, L., Sokhi, R., Solazzo, E., Tuccella, P., Unal, A., Vivanco, M. G., Hogrefe, C., and Galmarini, S.: Modelling black carbon absorption of solar radiation: combining external and internal mixing assumptions, Atmos Chem Phys, 19, 181-204, 10.5194/acp-19-181-2019, 2019.

Curtis, J. H., Riemer, N., and West, M.: A single-column particle-resolved model for simulating the vertical distribution of aerosol mixing state: WRF-PartMC-MOSAIC-SCM v1.0, Geosci. Model Dev., 10, 4057-4079, 10.5194/gmd-10-4057-2017, 2017.

Dentener, F., Kinne, S., Bond, T., Boucher, O., Cofala, J., Generoso, S., Ginoux, P., Gong, S., Hoelzemann, J. J., Ito, A., Marelli, L., Penner, J. E., Putaud, J. P., Textor, C., Schulz, M., van der Werf, G. R., and Wilson, J.: Emissions of primary aerosol and precursor gases in the years 2000 and 1750 prescribed data-sets for AeroCom, Atmospheric Chemistry and Physics, 6, 4321-4344, DOI 10.5194/acp-6-4321-2006, 2006.

Drinovec, L., Močnik, G., Zotter, P., Prévôt, A. S. H., Ruckstuhl, C., Coz, E., Rupakheti, M., Sciare, J., Müller, T., Wiedensohler, A., and Hansen, A. D. A.: The "dual-spot" Aethalometer: an improved measurement of aerosol black carbon with real-time loading compensation, Atmos. Meas. Tech., 8, 1965-1979, 10.5194/amt-8-1965-2015, 2015.

Du, H., Li, J., Chen, X., Wang, Z., Sun, Y., Fu, P., Li, J., Gao, J., and Wei, Y.: Modeling of aerosol property evolution during winter haze episodes over a megacity cluster in northern China: roles of regional transport and heterogeneous reactions of SO2, Atmospheric Chemistry and Physics, 19, 9351-9370, 10.5194/acp-19-9351-2019, 2019.

Emery, C., Liu, Z., Russell, A., Odman, M., Yarwood, G., and Kumar, N.: Recommendations on Statistics and Benchmarks to Assess Photochemical Model Performance, Journal of the Air & Waste Management Association (1995), 67, 10.1080/10962247.2016.1265027, 2016.

Fierce, L., Onasch, T. B., Cappa, C. D., Mazzoleni, C., China, S., Bhandari, J., Davidovits, P., Fischer, D. A., Helgestad, T., Lambe, A. T., Sedlacek, A. J., 3rd, Smith, G. D., and Wolff, L.: Radiative absorption enhancements by black carbon controlled by particle-to-particle heterogeneity in composition, Proceedings of the National Academy of Sciences of the United States of America, 117, 5196-5203, 10.1073/pnas.1919723117, 2020.

Fierce, L., Riemer, N., and Bond, T. C.: Toward Reduced Representation of Mixing State for Simulating Aerosol Effects on Climate, Bulletin of the American Meteorological Society, 98, 971-980, 10.1175/bams-d-16-0028.1, 2017.

Fuller, K. A., Malm, W. C., and Kreidenweis, S. M.: Effects of mixing on extinction by carbonaceous particles, Journal of Geophysical Research-Atmospheres, 104, 15941-15954, Doi 10.1029/1998jd100069, 1999.

Gao, M., Han, Z., Tao, Z., Li, J., Kang, J.-E., Huang, K., Dong, X., Zhuang, B., Li, S., Ge, B., Wu, Q., Lee, H.-J., Kim, C.-H., Fu, J. S., Wang, T., Chin, M., Li, M., Woo, J.-H., Zhang, Q., Cheng, Y., Wang, Z., and Carmichael, G. R.: Air quality and climate change, Topic 3 of the Model Inter-Comparison Study for Asia Phase III (MICS-Asia III) - Part 2: aerosol radiative effects and aerosol feedbacks, Atmospheric Chemistry and Physics, 20, 1147-1161, 10.5194/acp-20-1147-2020, 2020.

Hess, M., Koepke, P., and Schult, I.: Optical properties of aerosols and clouds: The software package OPAC, Bulletin of the American Meteorological Society, 79, 831-844, Doi 10.1175/1520-0477(1998)079<0831:Opoaac>2.0.Co;2, 1998.

Hu, K., Liu, D., Tian, P., Wu, Y., Li, S., Zhao, D., Li, R., Sheng, J., Huang, M., Ding, D., Liu, Q., Jiang, X., Li, Q., and Tao, J.: Identifying the Fraction of Core–Shell Black Carbon Particles in a Complex Mixture to Constrain the Absorption Enhancement by Coatings, Environ Sci Tech Let, 9, 10.1021/acs.estlett.2c00060, 2022.

Huang, X.-F., Peng, Y., Wei, J., Peng, J., Lin, X.-Y., Tang, M.-X., Cheng, Y., Men, Z., Fang, T., Zhang, J., He, L.-Y., Cao, L.-M., Liu, C., Zhang, C., Mao, H., Seinfeld, J. H., and Wang, Y.: Microphysical complexity of black carbon particles restricts their warming potential, One Earth, 10.1016/j.oneear.2023.12.004, 2023.

IPCC: Climate Change 2021: The Physical Science Basis. Contribution of Working Group I to the Sixth Assessment Report of the Intergovernmental Panel on Climate Change, Cambridge University Press, Cambridge, United Kingdom and New York, NY, USA, 2021.

Jacobson, M. Z.: Comment on "Radiative absorption enhancements due to the mixing state of atmospheric black carbon", Science, 339, 393, 10.1126/science.1229920, 2013.

Kang, Z., Ma, P., Quan, J., Liao, Z., Pan, Y., Liu, H., Pan, X., Dou, Y., Zhao, X., Cheng, Z., Wang, Q., Yuan, T., and Jia, X.: Mixing state of refractory black carbon in the residual layer over megacity, Atmospheric Environment, 295, 119558, 10.1016/j.atmosenv.2022.119558, 2023.

Li, J., Chen, X., Wang, Z., Du, H., Yang, W., Sun, Y., Hu, B., Li, J., Wang, W., Wang, T., Fu, P., and Huang, H.: Radiative and heterogeneous chemical effects of aerosols on ozone and inorganic aerosols over East Asia, The Science of the total environment, 622-623, 1327-1342, 10.1016/j.scitotenv.2017.12.041, 2018.

Li, J., Han, Z., Wu, Y., Xiong, Z., Xia, X., Li, J., Liang, L., and Zhang, R.: Aerosol radiative effects and feedbacks on boundary layer meteorology and PM2.5 chemical components during winter haze events over the Beijing-Tianjin-Hebei region, Atmospheric Chemistry and Physics, 20, 8659-8690, 10.5194/acp-20-8659-2020, 2020.

Li, M., Liu, H., Geng, G. N., Hong, C. P., Liu, F., Song, Y., Tong, D., Zheng, B., Cui, H. Y., Man, H. Y., Zhang, Q., and He, K. B.: Anthropogenic emission inventories in China: a review, Natl Sci Rev, 4, 834-866, 10.1093/nsr/nwx150, 2017.

Li, W., Shao, L., Zhang, D., Ro, C.-U., Hu, M., Bi, X., Geng, H., Matsuki, A., Niu, H., and Chen, J.: A review of single aerosol particle studies in the atmosphere of East Asia: morphology, mixing state, source, and heterogeneous reactions, Journal of Cleaner Production, 112, 1330-1349, 10.1016/j.jclepro2015.04.050, 2016.

Li, W., Riemer, N., Xu, L., Wang, Y., Adachi, K., Shi, Z., Zhang, D., Zheng, Z., and Laskin, A.: Microphysical properties of atmospheric soot and organic particles: measurements, modeling, and impacts, npj Climate and Atmospheric Science, 7, 65, 10.1038/s41612-024-00610-8, 2024.

Lin, P., Hu, M., Deng, Z., Slanina, J., Han, S., Kondo, Y., Takegawa, N., Miyazaki, Y., Zhao, Y., and Sugimoto, N.: Seasonal and diurnal variations of organic carbon in PM2.5 in Beijing and the estimation of secondary organic carbon, Journal of Geophysical Research: Atmospheres, 114, https://doi.org/10.1029/2008JD010902, 2009.

Liu, C., Chung, C., Yin, Y., and Schnaiter, M.: The absorption Ångström exponent of black carbon: From numerical aspects, Atmospheric Chemistry and Physics, 18, 6259-6273, 10.5194/acp-18-6259-2018, 2018.

Liu, D. T., Whitehead, J., Alfarra, M. R., Reyes-Villegas, E., Spracklen, D. V., Reddington, C. L., Kong, S. F., Williams, P. I., Ting, Y. C., Haslett, S., Taylor, J. W., Flynn, M. J., Morgan, W. T., McFiggans, G., Coe, H., and Allan, J. D.: Black-carbon absorption enhancement in the atmosphere determined by particle mixing state, Nat Geosci, 10, 184-U132, 10.1038/Ngeo2901, 2017.

Liu, D. T., He, C. L., Schwarz, J. P., and Wang, X.: Lifecycle of light-absorbing carbonaceous aerosols in the atmosphere, Npj Clim Atmos Sci, 3, 40, 10.1038/s41612-020-00145-8, 2020.

Liu, X., Ma, P.-L., Wang, H., Tilmes, S., Singh, B., Easter, R., Ghan, S., and Rasch, P.: Description and evaluation of a new four-mode version of the Modal Aerosol Module (MAM4) within version 5.3 of the Community Atmosphere Model, Geoscientific Model Development, 9, 505-522, 10.5194/gmd-9-505-2016, 2016.

Mann, G., Carslaw, K., Spracklen, D., Ridley, D., Manktelow, P., Chipperfield, M., Pickering, S., and Johnson, C.: Description and evaluation of GLOMAP-mode aerosol microphysics model for the UKCA composition-climate model, Geoscientific Model Development Discussions, 3, 10.5194/gmd-3-519-2010, 2010.

Matsui, H.: Black carbon simulations using a size- and mixing-state-resolved three-dimensional model: 1. Radiative effects and their uncertainties, Journal of Geophysical Research-Atmospheres, 121, 1793-1807, 10.1002/2015jd023998, 2016.

Matsui, H., Hamilton, D. S., and Mahowald, N. M.: Black carbon radiative effects highly sensitive to emitted particle size when resolving mixing-state diversity, Nature Communications, 9, 3446, 10.1038/s41467-018-05635-1, 2018.

Matsui, H., Koike, M., Kondo, Y., Fast, J., and Takigawa, M.: Development of an aerosol microphysical module: Aerosol Two-dimensional bin module for formation and Aging Simulation (ATRAS), Atmospheric Chemistry and Physics, 14, 10.5194/acp-14-10315-2014, 2014.

Mie, G.: Beiträge zur Optik Trüber Medien, Speziell Kolloidaler Metallösungen, Ann. Phys., 25, 377, 10.1002/andp.19083300302, 1908.

Mishchenko, M. I., Dlugach, J. M., Yanovitskij, E. G., and Zakharova, N. T.: Bidirectional reflectance of flat, optically thick particulate layers: an efficient radiative transfer solution and applications to snow and soil surfaces, Journal of Quantitative Spectroscopy & Radiative Transfer, 63, 409-432, Doi 10.1016/S0022-4073(99)00028-X, 1999.

Peng, J., Hu, M., Guo, S., Du, Z., Zheng, J., Shang, D., Levy Zamora, M., Zeng, L., Shao, M., Wu, Y. S., Zheng, J., Wang, Y., Glen, C. R., Collins, D. R., Molina, M. J., and Zhang, R.: Markedly enhanced absorption and direct radiative forcing

585   of black carbon under polluted urban environments, Proceedings of the National Academy of Sciences of the United States of America, 113, 4266-4271, 10.1073/pnas.1602310113, 2016.

Obiso, V. and Jorba, O.: Aerosol-radiation interaction in atmospheric models: Idealized sensitivity study of simulated short-wave direct radiative effects to particle microphysical properties, Journal of Aerosol Science, 115, 46-61, 10.1016/j.jaerosci.2017.10.004, 2018.

590   Paasonen, P., Kupiainen, K., Klimont, Z., Visschedijk, A., Denier van der Gon, H. A. C., and Amann, M.: Continental anthropogenic primary particle number emissions, Atmos. Chem. Phys., 16, 6823-6840, 10.5194/acp-16-6823-2016, 2016.

Qin, Y. M., Tan, H. B., Li, Y. J., Li, Z. J., Schurman, M. I., Liu, L., Wu, C., and Chan, C. K.: Chemical characteristics of brown carbon in atmospheric particles at a suburban site near Guangzhou, China, Atmos. Chem. Phys., 18, 16409-595   16418, 10.5194/acp-18-16409-2018, 2018.

Riemer, N., P. Ault, A., West, M., L. Craig, R., and H. Curtis, J.: Aerosol Mixing State: Measurements, Modeling, and Impacts, Reviews of Geophysics, 10.1029/2018RG000615, 2019.

Riemer, N., West, M., Zaveri, R. A., and Easter, R. C.: Simulating the evolution of soot mixing state with a particle-resolved aerosol model, Journal of Geophysical Research-Atmospheres, 114, 10.1029/2008jd011073, 2009.

600   Ran, L., Deng, Z. Z., Wang, P. C., and Xia, X. A.: Black carbon and wavelength-dependent aerosol absorption in the North China Plain based on two-year aethalometer measurements, Atmospheric Environment, 142, 132-144, 10.1016/j.atmosenv.2016.07.014, 2016.

Shen, W. X., Wang, M. H., Riemer, N., Zheng, Z. H., Liu, Y. W., and Dong, X. Y.: Improving BC Mixing State and CCN Activity Representation With Machine Learning in the Community Atmosphere Model Version 6 (CAM6), Journal of 605   Advances in Modeling Earth Systems, 16, 10.1029/2023MS003889, 2024.

Stevens, R., and Dastoor, A.: A Review of the Representation of Aerosol Mixing State in Atmospheric Models, Atmosphere, 10, 168, 10.3390/atmos10040168, 2019.

Sun, J., Xie, C., Xu, W., Chen, C., Ma, N., Xu, W., Lei, L., Li, Z., He, Y., Qiu, Y., Wang, Q., Pan, X., Su, H., Cheng, Y., Wu, C., Fu, P., Wang, Z., and Sun, Y.: Light absorption of black carbon and brown carbon in winter in North China Plain: 610   comparisons between urban and rural sites, The Science of the total environment, 770, 144821, 10.1016/j.scitotenv.2020.144821, 2021.

Toon, O. B., and Ackerman, T. P.: Algorithms for the calculation of scattering by stratified spheres, Appl Opt, 20, 3657-3660, 10.1364/AO.20.003657, 1981.

Tuccella, P., Curci, G., Pitari, G., Lee, S., and Jo, D. S.: Direct Radiative Effect of Absorbing Aerosols: Sensitivity to 615   Mixing State, Brown Carbon, and Soil Dust Refractive Index and Shape, Journal of Geophysical Research-Atmospheres, 125, 10.1029/2019JD030967, 2020.

Wang, J., Liu, D., Ge, X., Wu, Y., Shen, F., Chen, M., Zhao, J., Xie, C., Wang, Q., Xu, W., Zhang, J., Hu, J., Allan, J., Joshi, R., Fu, P., Coe, H., and Sun, Y.: Characterization of black carbon-containing fine particles in Beijing during wintertime, Atmos. Chem. Phys., 19, 447-458, 10.5194/acp-19-447-2019, 2019.

620 Wang, Y., Li, W., Huang, J., Liu, L., Pang, Y., He, C., Liu, F., Liu, D., Bi, L., Zhang, X., and Shi, Z.: Nonlinear Enhancement of Radiative Absorption by Black Carbon in Response to Particle Mixing Structure, Geophysical Research Letters, 48, 10.1029/2021gl096437, 2021a.

Wang, Y., Hu, R., Wang, Q., Li, Z., Cribb, M., Sun, Y., Song, X., Shang, Y., Wu, Y., Huang, X., and Wang, Y.: Different effects of anthropogenic emissions and aging processes on the mixing state of soot particles in the nucleation and

625 accumulation modes, Atmos. Chem. Phys., 22, 14133-14146, 10.5194/acp-22-14133-2022, 2022.

Wang, Y. Y., Pang, Y. E., Huang, J., Bi, L., Che, H. Z., Zhang, X. Y., and Li, W. J.: Constructing Shapes and Mixing Structures of Black Carbon Particles With Applications to Optical Calculations, Journal of Geophysical Research-Atmospheres, 126, e2021JD034620, 10.1029/2021JD034620, 2021b.

Wang, Z. F., Maeda, T., Hayashi, M., Hsiao, L. F., and Liu, K. Y.: A nested air quality prediction modeling system for urban

630 and regional scales: Application for high-ozone episode in Taiwan, Water Air and Soil Pollution, 130, 391-396, Doi 10.1023/A:1013833217916, 2001.

Wu, Y., Zhang, R., Tian, P., Tao, J., Hsu, S. C., Yan, P., Wang, Q., Cao, J., Zhang, X., and Xia, X.: Effect of ambient humidity on the light absorption amplification of black carbon in Beijing during January 2013, Atmospheric Environment, 124, 217-223, https://doi.org/10.1016/j.atmosenv.2015.04.041, 2016.

635 Wu, Y., Xia, Y., Zhou, C., Tian, P., Tao, J., Huang, R.-J., Liu, D., Wang, X., Xia, X., Han, Z., and Zhang, R.: Effect of source variation on the size and mixing state of black carbon aerosol in urban Beijing from 2013 to 2019: Implication on light absorption, Environmental pollution, 270, 116089, https://doi.org/10.1016/j.envpol.2020.116089, 2021.

Xie, C. H., Xu, W. Q., Wang, J. F., Wang, Q. Q., Liu, D. T., Tang, G. Q., Chen, P., Du, W., Zhao, J., Zhang, Y. J., Zhou, W., Han, T. T., Bian, Q. Y., Li, J., Fu, P. Q., Wang, Z. F., Ge, X. L., Allan, J., Coe, H., and Sun, Y. L.: Vertical

640 characterization of aerosol optical properties and brown carbon in winter in urban Beijing, China, Atmospheric Chemistry and Physics, 19, 165-179, 10.5194/acp-19-165-2019, 2019.

Xie, X., Hu, J., Qin, M., Guo, S., Hu, M., Ji, D., Wang, H., Lou, S., Huang, C., Liu, C., Zhang, H., Ying, Q., Liao, H., and Zhang, Y.: Evolution of atmospheric age of particles and its implications for the formation of a severe haze event in eastern China, Atmospheric Chemistry and Physics, 23, 10563-10578, 10.5194/acp-23-10563-2023, 2023.

645 Xu, P., Chen, Y., and Ye, X.: Haze, air pollution, and health in China, Lancet, 382, 2067, 10.1016/S0140-6736(13)62693-8, 2013.

Yang, W., Li, J., Wang, W., Li, J., Ge, M.-F., Sun, Y., Chen, X., Ge, B., Tong, S., Wang, Q., and Wang, Z.: Investigating secondary organic aerosol formation pathways in China during 2014, Atmospheric Environment, 213, 133–147, 10.1016/j.atmosenv.2019.05.057, 2019.

650 Yao, Y., Curtis, J. H., Ching, J., Zheng, Z., and Riemer, N.: Quantifying the effects of mixing state on aerosol optical properties, Atmos. Chem. Phys., 22, 9265-9282, 10.5194/acp-22-9265-2022, 2022.

Yu, F., and Luo, G.: Simulation of particle size distribution with a global aerosol model: contribution of nucleation to aerosol and CCN number concentrations, Atmos. Chem. Phys., 9, 7691–7710, 2009.

Yu, F., Luo, G., and Ma, X.: Regional and global modeling of aerosol optical properties with a size, composition, and mixing
655 state resolved particle microphysics model, Atmospheric Chemistry and Physics, 12, 5719-5736, 10.5194/acp-12-5719-2012, 2012.

Yu, P., Toon, O., Bardeen, C., Mills, M., Fan, T., English, J., and Neely, R.: Evaluations of Tropospheric Aerosol Properties Simulated by the Community Earth System Model with a Sectional Aerosol Microphysics Scheme, Journal of Advances in Modeling Earth Systems, 7, 10.1002/2014MS000421, 2015.

660 Yus-Díez, J., Bernardoni, V., Močnik, G., Alastuey, A., Ciniglia, D., Ivančič, M., Querol, X., Perez, N., Reche, C., Rigler, M., Vecchi, R., Valentini, S., and Pandolfi, M.: Determination of the multiple-scattering correction factor and its cross-sensitivity to scattering and wavelength dependence for different AE33 Aethalometer filter tapes: a multi-instrumental approach, Atmos. Meas. Tech., 14, 6335-6355, 10.5194/amt-14-6335-2021, 2021.

Zaveri, R. A., Barnard, J. C., Easter, R. C., Riemer, N., and West, M.: Particle-resolved simulation of aerosol size,
665 composition, mixing state, and the associated optical and cloud condensation nuclei activation properties in an evolving urban plume, Journal of Geophysical Research-Atmospheres, 115, 10.1029/2009jd013616, 2010.

Zhang, H., Guo, H., Hu, J., Ying, Q., and Kleeman, M. J.: Modeling atmospheric age distribution of elemental carbon using a regional age-resolved particle representation framework, Environmental science & technology, 2018.

Zhang, Y. T., Liu, H., Lei, S. D., Xu, W. Y., Tian, Y., Yao, W. J., Liu, X. Y., Liao, Q., Li, J., Chen, C., Sun, Y. L., Fu, P. Q.,
670 Xin, J. Y., Cao, J. J., Pan, X. L., and Wang, Z. F.: Mixing state of refractory black carbon in fog and haze at rural sites in winter on the North China Plain, Atmospheric Chemistry and Physics, 21, 17631-17648, 10.5194/acp-21-17631-2021, 2021.

Zhao, G., Shen, C., and Zhao, C.: Technical note: Mismeasurement of the core-shell structure of black carbon-containing ambient aerosols by SP2 measurements, Atmospheric Environment, 243, 117885,
675 https://doi.org/10.1016/j.atmosenv.2020.117885, 2020.

Zhao, G., Tan, T., Hu, S., Du, Z., Shang, D., Wu, Z., Guo, S., Zheng, J., Zhu, W., Li, M., Zeng, L., and Hu, M.: Mixing state of black carbon at different atmospheres in north and southwest China, Atmospheric Chemistry and Physics, 22, 10861-10873, 10.5194/acp-22-10861-2022, 2022.

Zhao, G., Tan, T., Zhu, Y., Hu, M., and Zhao, C.: Method to quantify black carbon aerosol light absorption enhancement
680 with a mixing state index, Atmos. Chem. Phys., 21, 18055-18063, 10.5194/acp-21-18055-2021, 2021.

Zhao, P., Dong, F., Yang, Y., He, D., Zhao, X., Zhang, W., Yao, Q., and Liu, H.: Characteristics of carbonaceous aerosol in the region of Beijing, Tianjin, and Hebei, China, Atmospheric Environment, 71, 389-398, https://doi.org/10.1016/j.atmosenv.2013.02.010, 2013.

685 Zheng, H., Kong, S., Chen, N., and Wu, C.: Secondary inorganic aerosol dominated the light absorption enhancement of black carbon aerosol in Wuhan, Central China, Atmospheric Environment, 119288, https://doi.org/10.1016/j.atmosenv.2022.119288, 2022.

Zheng, G. J., Duan, F. K., Su, H., Ma, Y. L., Cheng, Y., Zheng, B., Zhang, Q., Huang, T., Kimoto, T., Chang, D., Pöschl, U., Cheng, Y. F., and He, K. B.: Exploring the severe winter haze in Beijing: the impact of synoptic weather, regional transport15-2969-2015, 2015.

690 Zhou, C. H., Gong, S., Zhang, X. Y., Liu, H. L., Xue, M., Cao, G. L., An, X. Q., Che, H. Z., Zhang, Y. M., and Niu, T.: Towards the improvements of simulating the chemical and optical properties of Chinese aerosols using an online coupled model – CUACE/Aero, Tellus Series B-chemical Physical Meteorology, 64, 91-102, 2012.